

CHAPTER 59. INDOOR AIRFLOW MODELING

WHEN trying to determine best design practices for specific indoor spaces, building designers may encounter uncertainties regarding control of airflow, indoor air quality, thermal comfort, or heat transfer. A design may need to fulfill specialized requirements, such as reducing contaminant transport across building zones in a hospital or providing the most energy-efficient configuration for cooling in a cutting-edge data center. Evaluating performance of these complex and highly engineered designs is often beyond the ability of the tables, rules of thumb, and simple formulas given in the *ASHRAE Handbook*. In these situations, computer models allow designers to quantitatively evaluate multiple designs quickly and with a good degree of accuracy. This chapter expands on the general guidance of [Chapter 13 in the 2021 ASHRAE Handbook—Fundamentals](#), with the addition of industry-specific advice and examples to aid designers in modeling indoor applications. Although this chapter is intended to be a fast-start guide for modeling indoor airflow, engineers should have a basic understanding of fluid mechanics and the modeling principles described in [Chapter 13 of 2021 ASHRAE Handbook—Fundamentals](#).

1. PRELIMINARY CONSIDERATIONS

Although indoor airflow modeling provides engineers with unparalleled insights and visual design aids, the resulting model is only as good as the specified inputs and assumptions. An engineer must be cautious in selecting modeling parameters and carefully examine the simulation results before making any design decision. Circumspection is especially needed when simulation predictions do not conform to standard design practice.

First determine the scope of the domain (the physical extent of the simulated space) of a model; for most cases, this is a discrete indoor space, although it is possible to model a larger domain including multiple spaces or, conversely, a small domain containing only a subsection of a space. Next, determine the intent, or the desired output from the model. Local air velocities and temperatures or airflow rate into/out of a space are often the primary interests, but it is common to also include parameters such as relative humidity and pollutant concentration or application-specific derived data. With the modeling goals in mind, it is possible to provide appropriate inputs and select methodologies consistent with the desired quality of results.

The two methods featured in this chapter are computational fluid dynamics (CFD) and multizone (MZ) modeling, described in detail in [Chapter 13 of the 2021 ASHRAE Handbook—Fundamentals](#). CFD is typically used if a detailed airflow pattern/thermal comfort/indoor air quality analysis of a single space is desired. If only the aggregated zone information is important and determining the interaction between multiple spaces is desired (e.g., average airflow rates in individual rooms, spread of a contaminant through an entire building), the multizone method provides satisfactory results without the significant computational investment and complicated setup of CFD.

2. COMPUTATIONAL FLUID DYNAMICS (CFD)

CFD methods simulate the detailed airflow distribution and related physical phenomena in a space and provide detailed information, such as temperature and relative humidity, at specific points. However, due to the relatively high computational cost, the size and geometric complexity of the space that can be modeled is limited by the computational resources available. Practitioners who plan to use CFD must weigh the computational requirements against the expected accuracy of the simulated results to determine the appropriate level of detail to implement in the CFD model. Detailed background and theoretical development can be found in [Chapter 13 of the 2021 ASHRAE Handbook—Fundamentals](#). This section provides only basic guidelines for modeling indoor airflow and associated attributes.

2.1 TERMINOLOGY

Terms and definitions in this section are neither comprehensive nor specific to any software packages. However, these terms should be easily recognized and applicable to any CFD software platform.

Domain. The specific space to be modeled in the CFD simulation. Typically, it is a single discrete space in a building, but it may be as large as several blocks of a street, or limited to only a specific region within a room.

Geometry. The physical geometry normally includes both the extent of the solution domain and the physical objects in it. The physical objects may form an integral part of the CFD model or may be excluded, depending on the intent of the computational model.

Mesh. Mesh, also called **grid**, is the discretized representation of the geometry. For CFD software to conduct its simulation, any geometry must be broken into a large number of small pieces or elements. The process of breaking up

the geometry is called *meshing*, *gridding*, or *grid generation*.

Cell. This is the smallest individual unit of a mesh.

Mesh/cell type. Different cell geometries are used, and are typically basic geometric shapes. *Tetrahedral* (four faces) and *hexahedral* (six faces) are two common types. A *polyhedral* (shape-independent) mesh uses a collage of different shapes.

Mesh/cell organization. Structured grids are identified by regular connectivity. The simplest form is a single, block structured Cartesian mesh, where the cells form a hexahedral mesh containing only rectangular brick-shaped elements, with every face in a plane aligned with two of the Cartesian axes. The lines of such a mesh extend through the entire solution domain. An unstructured grid is identified by irregular connectivity. More complex meshing strategies often use unstructured meshes because the neighboring cell's data is no longer guaranteed to be the next cell in a three-dimensional matrix, and cell connectivity also has to be stored.

Aspect ratio. A measure of the stretching of a cell. This compares how similar in length a cell's sides are. Highly stretched cells are typically avoided, because this can distort simulation results.

Cell growth rate. A measure of how rapidly the size of cells changes for a given region. High growth rate is typically avoided because flow characteristic details might be lost.

Boundary conditions. A boundary condition is a surface or volume where known or estimated properties can be applied. These properties are the input parameter for CFD simulations.

Source/sink. Sources and sinks are specific boundary conditions that provide a net gain or a net loss of a specific quantity of mass, heat, or momentum.

Residual error. Residual is one of the fundamental measures of an iterative solution's convergence: it directly quantifies the error in the solution of the system of equations. In a CFD analysis, the residual measures the local imbalance of a conserved variable in each control volume.

2.2 OVERVIEW OF CFD SIMULATION

Following are the seven steps generally applicable to modeling indoor airflow in CFD.

1. **Geometry generation.** A physical model of the domain is generated from scratch or converted from an existing architectural model. Whether the geometry includes both the fluid and solid portions depends on the scope of the analysis. (In this chapter, a **fluid** is defined as a substance that deforms continuously in response to shear stress, and a **solid** is a substance with a fixed shape.) Generally, the fluid portion is sufficient for most types of analysis. The geometric model should capture all essential features of the space such as flow obstructions (e.g., furniture, equipment), air supply/return devices, and heat sources/sinks (e.g., exterior glazing, occupants, equipment). The geometric model should be kept as simple as possible, while still maintaining sufficient accuracy and satisfying the intent of the analysis.
2. **Mesh generation.** Mesh creation may occur in or outside of the CFD software package. Regardless of what tool is used, the meshing process should generally follow this outline:
 - a. Define desired outcome of simulation to reach meshing decisions.
 - b. Decide mesh/cell types. This selection usually follows the geometric shape of the 3D model. In buildings, due to the rectangular cubic nature of the space, the hexahedral mesh is often used. However, other types of mesh could be more suitable if geometry requirements exceed the nature of hexahedral mesh.
 - c. Determine cell size and number. Computational cost increases with number of cells. Though increasing the number of cells by decreasing cell size typically improves the accuracy of CFD simulation results, there is a practical limit on the number of cells for a given project due to both computational resources and time constraints.
 - d. Define the region of refinement. Given the practical limit on number of cells to be used, the engineer should focus on the optimal distribution of cell size for a given scenario, with finer cells used for regions of interest or near surfaces or regions where large gradients are expected.
 - e. Select an appropriate aspect ratio. An aspect ratio close to 1 ensures that the shape of the cells does not distort simulation results by ignoring the influence on details caused by the stretched dimension.
 - f. Transition/growth rate needs to be gradual. If the transition from small cell to large cell is abrupt, there could be loss in detail, impacting the resulting flow pattern.
 - g. Wall boundary layers often require additional mesh refinement due to the interaction between solid and fluid.

Meshing is generally an iterative process, and the most suitable number and distribution of cells can sometimes only be identified after the simulation results have been verified. The included simulation examples provide some guidelines on the process for specific scenarios.

3. **Model/solver selection.** CFD is the process to iteratively solve the Navier-Stokes (NS) equations, which are the basic governing equations for a viscous, heat-conducting fluid. CFD software typically includes the option to select various physical/mathematical simulation models to help solve the NS equations. Some of the possible model parameters include the following:
- *Steady-state and transient simulation.* Indoor environments are inherently unsteady, but a steady-state (SS) or a quasi-steady state (QSS) simplification can usually represent the bulk airflow pattern well. Hence, one of the very first decisions in a CFD simulation workflow is whether to conduct the simulation in SS or transient modes. An SS model simulates a snapshot of a moment in time. A transient model allows engineers to investigate flow characteristics that change over time.
 - *Fluid properties of air.* Although many fluid properties (e.g., density, pressure, viscosity) can be changed, usually the most important parameter is the fluid density, because it can alter the method of fluid movement calculation (see Buoyancy model).
 - *Buoyancy model.* When incompressible fluid is assumed (due to minimal change in pressure and temperature), density remains constant and buoyancy might be ignored or handled separately (through methods such as the Boussinesq approximation [Gray and Giorgini 1976]). Otherwise, an ideal-gas or real-gas model should be used.
 - *Energy model/equation.* The energy model accounts for the energy/heat transfer between the cells in CFD, and subsequently, the temperature for each cell. Some CFD software allows decoupling of energy model from the physical model for isothermal analysis. For most cases, due to local heat sources and higher/lower air temperature from the supply registers, the energy model should be enabled and coupled with a flow model.
 - *Thermal radiation model.* The indoor environment may include large surface-to-surface temperature difference or significant exposure to sunlight. In those cases, if forced-convection fluid transport is not dominant, a radiation model might provide a more accurate assessment of heat transfer in the domain, in addition to the conduction/convection-based transport in CFD.
 - *Turbulence model.* Because the typical cell size used in CFD is too large to directly simulate fluid-flow turbulence, turbulence models are used. Specific modeling techniques, including Reynolds-averaged Navier-Stokes (RANS) and large eddy simulation (LES), are discussed in [Chapter 13 of the 2021 ASHRAE Handbook—Fundamentals](#). The importance of selecting an appropriate turbulence model cannot be overstated. This has a significant impact on the modeled physics and the accuracy of the simulation. Due to their reasonable accuracy and low computational cost, RANS models (such as RANS k - ϵ RNG) are widely used. Relevant literature should be consulted for more guidance on choosing the appropriate turbulence model (e.g., Chen et al. [2010]). Examples of such selections can be found in the section on Multizone Simulation Method.
 - *Species model.* The species model is used when different types of fluids (in most cases, fluids other than air), each with distinct fluid properties, are combined. One application of such a model is to track gaseous pollutants (e.g., volatile organic compounds, [VOCs]) in an indoor space.
4. **Boundary conditions.** Every surface in the CFD model provides a parameterized boundary to the fluid space that is simulated, and the conditions/inputs for these surfaces must be set. Several common boundaries typically encountered in indoor airflow simulations are as follows:
- *Wall.* For most CFD software packages, any defined solid/surface has the default classification of wall, which usually indicates a solid, nonpermeable, no-slip surface. A wall can be slip or nonslip and/or have a roughness parameter associated with the surface, which can affect the turbulence simulation in the fluid region. In the case of the solid interacting with the fluid in a simulation, additional mechanisms may be introduced at the wall boundary. The interaction might include heat transfer, mass transfer, and chemical reactions.
 - *Inlet.* A surface set to inlet classification allows fluid flow into the simulation domain. The property of this flow can be defined by its velocity, direction, pressure, or flow rate. In the case of multiphase or multicomponent fluid simulation, the inlet definition might include the exact mixture of the fluid. The most common examples for an indoor inlet are the HVAC diffusers (as investigated by Srebric and Chen [2001]) or opened windows.
 - *Outlet.* This type of boundary allows fluid flow out of the simulation domain. Unlike an inlet, this boundary often does not require variables to be defined, because flow exiting the outflow boundary is outside of the simulation domain. In most cases, only hydrodynamic variables (pressure or velocity) need to be defined at an outlet. The most common example for an outlet in indoor airflow simulations is the return in an HVAC system.
 - *Source/sink.* Source and sink allow the specification of a flux of a specific quantity of interest. In most simulations, energy source/sink of the domain might be specified as a heat flux on a given surface or volume. In a multispecies simulation, injection or removal of gas or particles are treated as mass flux. When a mechanism that impacts the flow field is needed, artificial momentum flux might be applied.

5. **Solution convergence.** Because the CFD solution process is iterative, the solution must converge to a specified tolerance to be considered complete. If the solution has not met such criteria, the simulation results are usually considered inaccurate and insufficient for design purposes. Although some guidelines exist for when a solution is considered converged, there is no single definition. In general, convergence is usually judged by examining three solution parameters:
 - *Residuals of the equations being solved for the specific simulation* (e.g., momentum, mass, energy, species). These must fall below a certain tolerance before a solution is considered converged. The tolerance criteria are usually based on the physical property and the scale of defined problem.
 - *Global imbalance of the conserved quantities* (e.g., mass, momentum, energy). For steady-state simulations, the amount of mass, momentum, and heat going into a domain must be equal to that exiting the domain. The imbalance between the two must again fall below a specified tolerance for a solution to be considered converged.
 - *A specific variable in a region of interest.* Very roughly defined, when the variable of interest stops changing as the solution progresses, the simulation can be considered converged. For an indoor airflow simulation, examples are air temperature or velocity at specific monitor points. Guidelines on specific convergence criteria are discussed in the examples in the section on Multizone Simulation Method.
6. **Post processing.** Post processing takes the CFD solution at each cell and provides an easy-to-understand visualization in colorful and/or animated format. For example, a plane might be created in a simulation to bisect an entire simulation domain in order to display temperature profile/contour of the desired location. For reference, each of the cases in the section on CFD Examples includes specific visualization (i.e., post processing) unique to a given problem.
7. **Validation.** Even with simulations conducted with great care, results can still be incorrect due to unforeseen errors or poor assumptions. It is important to verify the results with domain knowledge or previous results that can be used as validation for the CFD simulation. Some sources of validation include published research articles, verified case studies, and previously designed projects.

3. CFD EXAMPLES

In this section, several real-world examples created by expert computational dynamics users demonstrate the use of simulations in buildings and indoor environments. Due to the diverse subject interests of contributors, the details vary. However, key information, including geometry and mesh construction, input parameters and boundary conditions, and solution convergence criteria, is included for all of the examples.

3.1 SIMPLE OFFICE WITH DIFFUSERS AND RETURNS

This example involves a typical office space with multiple cubicles, where supply air is delivered through ceiling diffusers, and return air enters through a grille on a wall. The purpose of this CFD simulation is to determine, under a steady-state (SS) assumption, the air characteristics (temperature and velocity) near the office workers seated in these cubicles. The SS assumption is used here because the workers often remain stationary for long periods of time, and the airflow characteristics do not vary significantly (flow rate and temperature of the air and surface remain steady). The following are specifications made for this simulation and the key parameters used, with a short discussion on the reasoning behind the decisions. Because this is the first example, some steps are explained in more detail with additional comments. This level of explanation is not repeated in the subsequent examples, but the considerations noted still apply.

Geometry Generation

As seen in [Figure 1](#), the geometry is generated to represent the office with cubicles. Note that the furniture, desks, and workers are modeled with very simplified geometry. This is common in indoor CFD simulation, because the primary interest is often the bulk air movement and temperature, and the microenvironment near objects and human bodies is of less importance. Consequently, the small-scale features and curvatures of the room objects can be overlooked. This particular office space geometry is generated using a CAD tool included in a commercial CFD package. However, it might be simpler for a practitioner to generate 3D geometry in an external CAD tool, especially if complex shapes and curvatures are required.

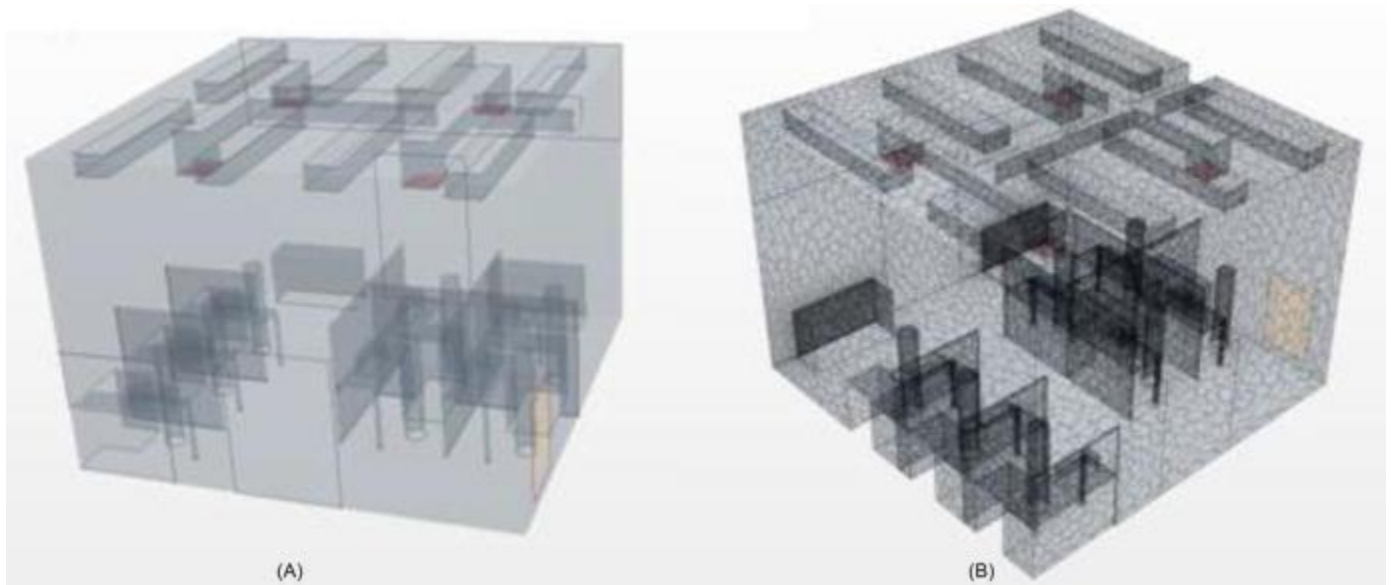


Figure 1. (A) Geometry and (B) Mesh

Mesh Generation

Part B of [Figure 1](#) displays the mesh generated for the office once the geometry is finalized. The base size of cells in the room might be relatively large depending on the complexity of the flow regime, but a grid independence test should be conducted to determine that a balance between calculation time and accuracy has been achieved. In this case, a base cell size of 11.8 in. (roughly the size of the diffuser opening) is used for the automatic mesh generator. Polyhedral mesh is used here to reduce amount of mesh manipulation required (compared to hexahedral mesh). There are additional refinements near the region of interests, such as the inlet, the heat flux sources (lights, computers), and near the occupants. In this case, a 10% base cell size is used to refine the region near the occupants, in the interest of comfort level. The 11.8 in. base size was also checked for grid independence, where smaller base size did not yield a change in results in monitor points near the occupants (due to the refinement, the cell size is roughly 1 in. near the occupants, hence it is sufficient for the simulation). This cell size results in roughly 50,000 cells in the simulation domain, a number that can be accommodated by typical personal computers.

Solver and Models

RANS with a $k-\varepsilon$ turbulence model (Chen et al. 2010) is selected because bulk flow near the occupants is the primary interest. Due to the heat flux in the room (see the section on Boundary Conditions), the flow energy coupled solver is used to determine the buoyancy aspect of the driving force in addition to the forced convection from the diffuser. For the same reason, the simulation assumes ideal gas (or real gas if a specific property is known) due to the small temperature and pressure variance in the domain.

Boundary Conditions

The specific boundary conditions for this example are the inlets, outlets, and heat sources in the room. The other boundary is a simple wall assumed to be no-slip. The outlet is a simple pressure outlet condition with a relative pressure of 0 in. of water compared to the room pressure (just upstream of the outlet) This is due to the inlet already providing the flow driving force, and results in a negative pressure at the outlet. The heat sources (people, computers, and lights) are given specific heat fluxes on their corresponding surfaces (see [Chapter 18 of the 2021 ASHRAE Handbook—Fundamentals](#)):

- Occupants: 170 Btu/h (sensible only)
- Lights: 102 Btu/h (single fluorescent tube)
- Computers: 170 Btu/h (nominal power consumption)

The supply diffuser model requires special consideration, because the inlet has a dominant influence on the room airflow pattern and velocity. Unlike the return/outlet, the supply/inlet must have both direction and magnitude in order to establish a correct flow field for the simulation. [Figure 2](#) shows an example of using the momentum method (Srebric and Chen 2002) to model the square louver diffuser in this problem.

The diffuser momentum method was chosen because, if the square diffuser supply for the office was left as a square hole without any additional information beyond the designed flow rate, this inlet boundary condition would be assigned

to a specific pressure differential or velocity inlet normal to the opening. This normal assumption is correct in terms of providing airflow rate into the room, but the initial velocity direction and subsequent flow pattern are completely incorrect: a diffuser would spread out the supply air for good mixing, whereas a square-hole inlet model generates a column of air with downward velocity. In [Figure 2](#), the square inlet is divided into 16 smaller inlets, each assigned with a different direction and velocity magnitude, in an attempt to replicate the dispersion airflow field from the diffuser. The resulting airflow pattern should follow the diffuser manufacturer data (throw/spread) or any experimental data available. Supply air temperature was set to 57°F, a typical value in U.S. office buildings.

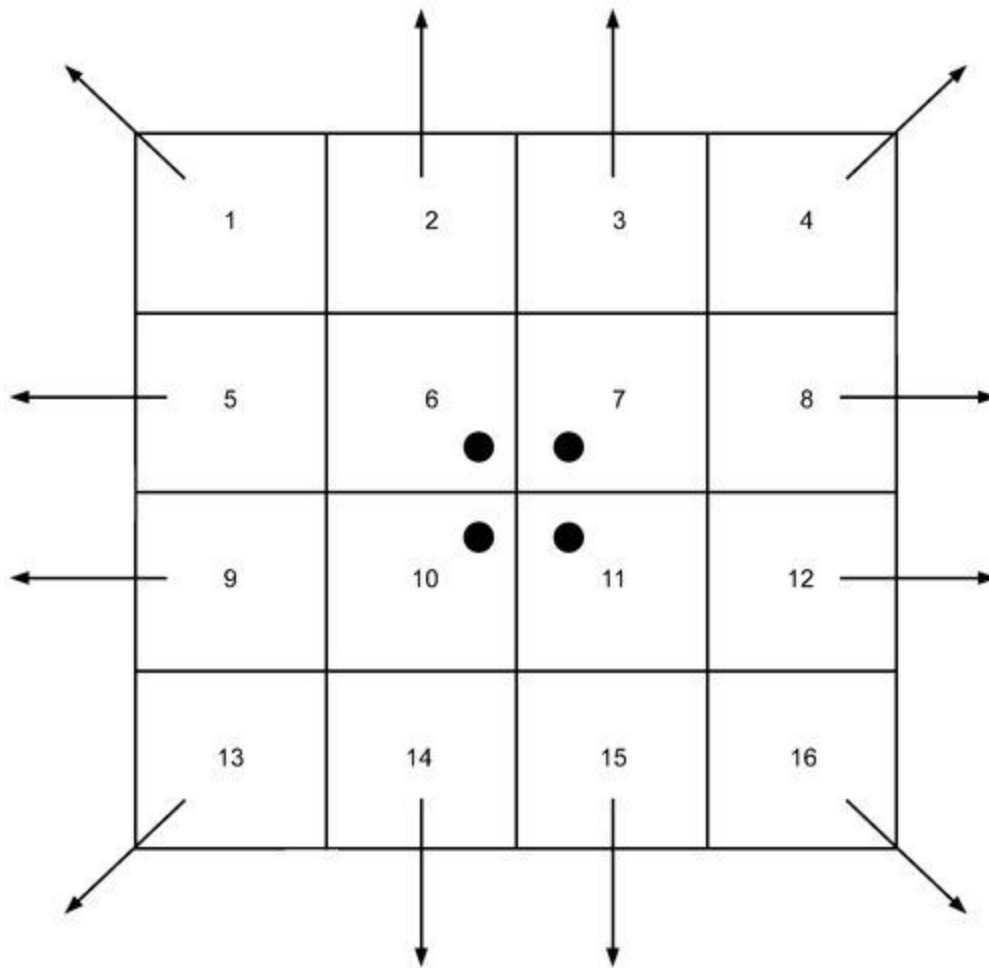


Figure 2. Illustration of Momentum Method for Inlet Model

In this method, because the air velocity and direction of multiple inlets are used, it is important to verify whether the total airflow rate from the inlets still represents the intended flow rate from the diffuser. If the momentum method is not applicable, Srebric and Chen (2011) also provide alternative diffuser modeling methods.

Convergence

Convergence of the CFD solution was achieved by monitoring the solution residuals as well as several temperature monitor points in various part of the room ([Figure 3](#)). In this case, the solution's mass and momentum equation residuals stabilized and dipped below 1×10^{-4} at roughly 450 iterations, and the temperatures stabilized at about 700 iterations. Selection of 1×10^{-4} in the continuity, momentum, and turbulence equation residuals is a typical rule of thumb for indoor CFD simulations, but 1×10^{-6} and 1×10^{-5} are recommended for the energy and species equations, respectively. These convergence tolerance metrics should be accompanied by stabilization of the solution variables. This stabilization indicates that a steady-state flow solution has emerged and the solution has been determined to be converged.

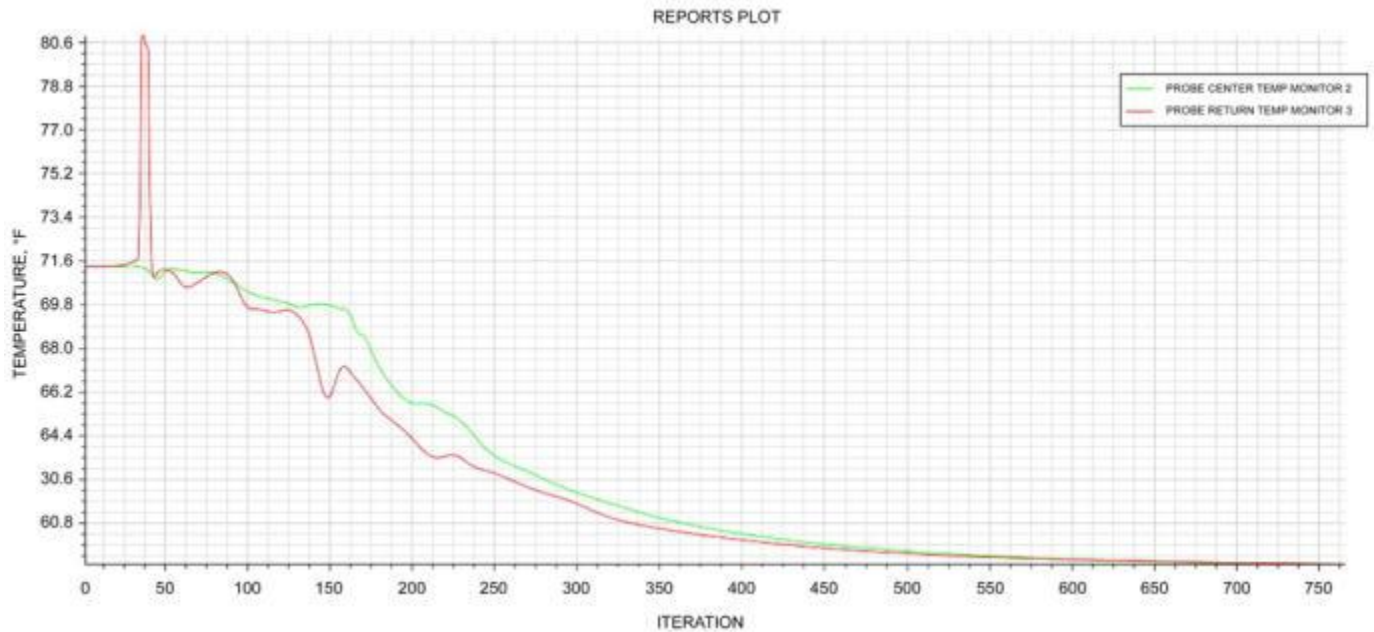


Figure 3. Temperature over Iteration Indicates Steady-State Convergence

Post Processing and Results

To display the simulation results, two planes were used to show the solution contours near the occupants, displaying the air temperature and air velocity (Figure 4). A horizontal cut plane at head level of the sitting occupants demonstrates breathing zone quantities, and the vertical cut plane through the diffusers demonstrates inlet flow regime.

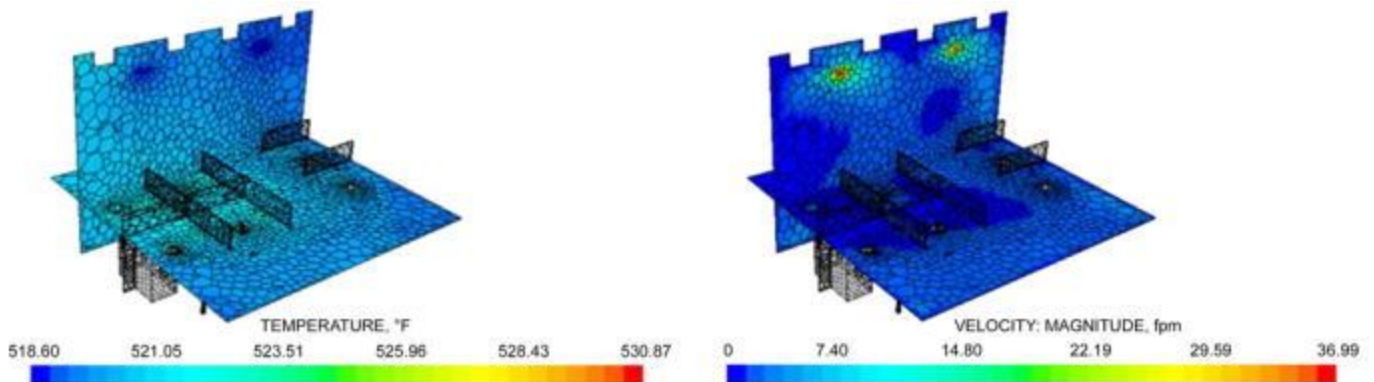


Figure 4. Temperature and Velocity Results from Simulation Shown in Two Planes Bisecting Region of Interest

Results

The goal of the simulation was to determine whether the temperature and air velocity meet the ASHRAE comfort requirements. Per ASHRAE *Standard* 55, it is evident the velocity did not reach the level of a noticeable cold drift, and temperature near occupants is well within the ASHRAE comfort zone. Hence, this particular design fulfills the comfort criteria.

3.2 CHILLED BEAM

Use of passive (without fans) cooling applications in buildings has been on the rise. However, without a specific airflow rate from a HVAC fan system, it is difficult to design the system to satisfy specific thermal comfort and moisture control criteria. The purpose of this CFD model is to investigate the performance of the chilled-beam design by analyzing condensation risk on the windows as well as thermal comfort and ventilation effectiveness in the space in heating mode. The following is a discussion of the various modeling decisions made for this specific case and the reasoning behind them.

Geometry of Open Office with Chilled Beams

The modeled section of the open office is a 1250 ft² space with a 9 ft high ceiling, and exterior windows. The office has cubicle desks with partitions and cabinets (as well as computers). This section of the office is conditioned with six two-way chilled beams in the ceiling, and return air is assumed to leave through an opening on the back wall ([Figure 5](#)).

[Figure 5](#) is a simplified representation of the gross geometry of the office. The geometric features are

- Furniture (e.g., desks, cabinets, and cubicle partitions)
- Simplified occupants
- Computers, broken up into a monitor and a tower
- Windows, which include some details of the mullions
- Chilled beam discharge slots (inlet)
- Chilled beam induction face (outlet)
- Return opening on back wall (outlet)

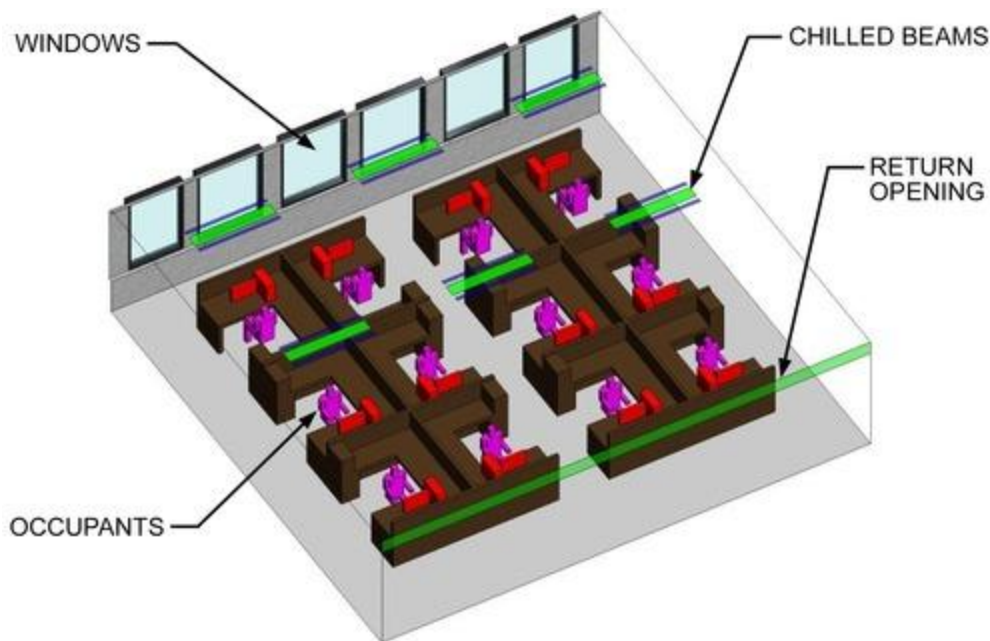


Figure 5. Office CFD Model: Simplified Geometric Model

Because the purpose of the model is to study bulk airflow and temperature distributions, simplicity is key when representing these features. Although box representations are used for all furniture and computers in the space, extra detail has been added to increase the fidelity of the simulation. For example, the spaces under the desks are included in the model, and the computers are split into parts (monitor and tower). This is not generally required, but was done to more accurately capture the thermal plumes from the occupants and the equipment in the space. Because there are only 12 occupants, more refined models of the occupants are used, although simplified models such as cylinders would have also been acceptable. These specific cuboid models include the arms, legs, and a head, while retaining the total surface area of an average-sized, seated adult male (see [Chapter 9 of the 2021 ASHRAE Handbook—Fundamentals](#)). When modeling heat/contaminant sources (e.g., occupants), the surface area of the simplified representation is very important, because it determines the temperature of the surface when a heat flux boundary condition is specified and vice versa. The windows in the model include some details of the mullions, because one of the purposes of the CFD model is to study condensation risk. Geometric representations of the chilled beams and returns depend on the modeling approach as well as the desired level of accuracy. The chilled-beam model is described in detail in the section on Boundary Conditions.

Mesh Generation

A snapshot of the computational mesh in a horizontal and vertical plane is shown in [Figure 6](#). A tetrahedral mesh is used in this example; it can efficiently handle complex geometries and is less sensitive to random changes in flow direction like the hexahedral mesh. It is also less labor intensive to generate for the geometry used in this example. Local mesh refinement is used around the various geometric features mentioned in the Overview of CFD Simulation Process section, with particular attention paid to local refinement around the heat sources (to capture thermal plumes),

as well as the discharge slots of the chilled beams (to capture the jets) and, to a lesser extent, the returns. Mesh refinement perpendicular to all surfaces in the model is used to capture the thermal and hydrodynamic boundary layers. For the current turbulence model, 12 layers of prismatic elements are used at the walls, with a dimensionless wall distance of $y^+ < 2$ for the first layer. In this simulation, a global mesh size of 5 in. is used, whereas mesh sizing of 2 in. is used around the computers, and 1 in. for the return/induction opening and the occupants. A mesh size of 1 in. is used on and around the discharge slots of the chilled beams to better capture the spread of the supply jet along the ceiling. A mesh growth ratio of 1:1 is used around the chilled-beam discharge slots, occupants, and computers, to ensure that this mesh refinement smoothly merges into the larger cell size of the room.

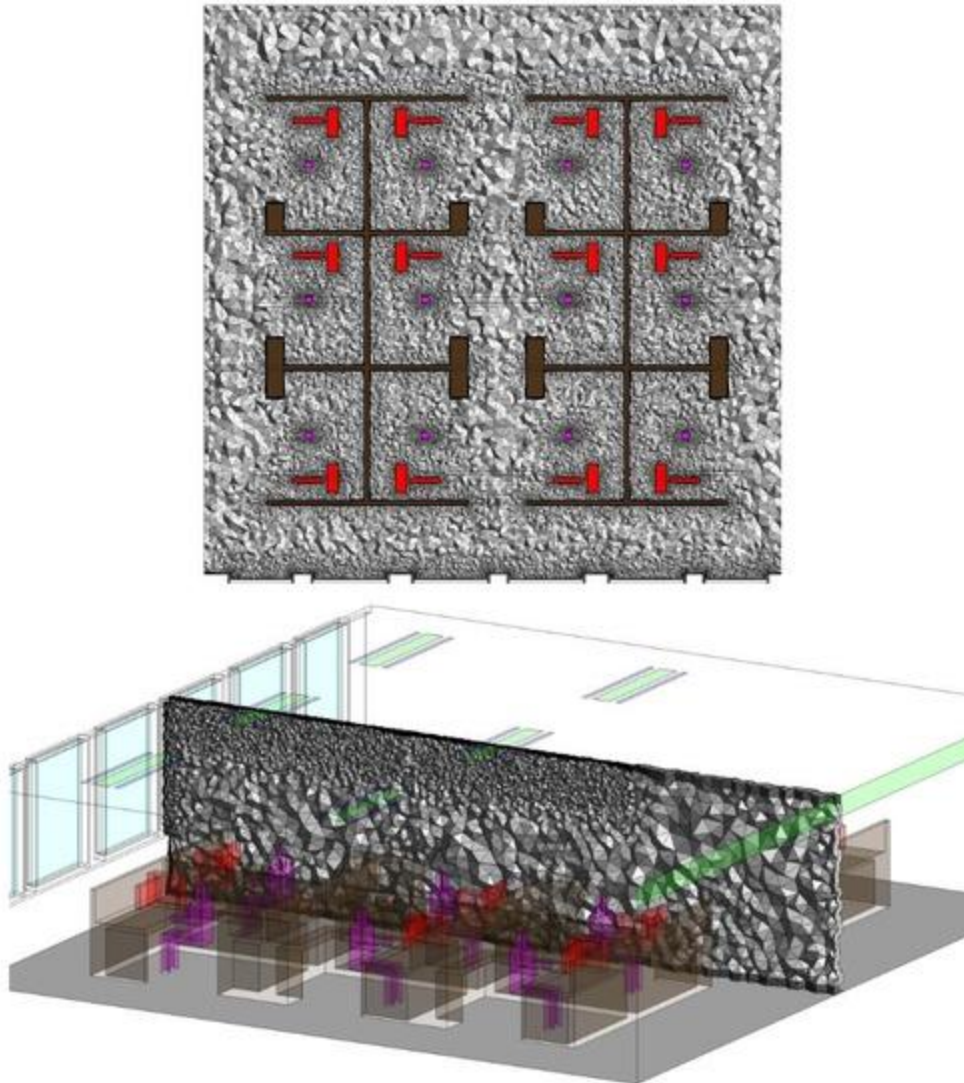


Figure 6. Classroom CFD Model: Computational Mesh Resolution at Vertical and Horizontal Planes

Boundary Conditions

The boundary conditions for this example are

- **Return opening** (back wall): No relative pressure, temperature, scalars, and turbulence quantities are extrapolated from the solution (do not need to be specified).
- **Windows:** Specified with a convective heat flux to model heat conduction through the glass.
- **Occupants:** Specified with radiant and convective heat flux, with 60% of the total heat gain being radiant and 40% being convective (see Table 1 in [Chapter 18 of the 2021 ASHRAE Handbook—Fundamentals](#)).
- **Lights:** Specified with radiant and convective heat flux (80/20% radiant/convective split) (see [Chapter 18 of the 2021 ASHRAE Handbook—Fundamentals](#)); boundary condition applied to entire ceiling.
- **Computers:** Specified with a radiant and a convective heat flux, with 15% of the total heat gain being radiant and 85% being convective (see Tables 8 and 11 in [Chapter 18 of the 2021 ASHRAE Handbook—Fundamentals](#)).

All radiation heat fluxes are assumed to be isotropic (independent of direction). The chilled-beam model itself is worth discussing in more detail. Specification of this boundary condition is divided into two parts: the discharge opening and the induction opening. To specify both, the following performance metrics of the chilled beam are required:

- Induction ratio K_{in}
- Primary airflow rate q_p
- Primary supply air temperature T_p
- The sensible capacity of cooling coil Q_{coil} at the specified primary airflow rate
- Discharge angle (can be assumed if not available)

The induction opening is specified as an outlet boundary with a mass flow rate equal to the total volume of air induced by the chilled beam $q_p K_{in}$. Velocity measurements across the induction face of chilled beams show that the induction velocity varies very little, making a uniform velocity assumption reasonable. The discharge opening is specified as an inlet boundary with the total volume of air (induced + primary, $q_p [K_{in} + 1]$) set at the specified discharge angle. In the current case, the discharge angle is set to 15° and is based on smoke videos of the chilled beam from the manufacturer. The correct discharge is important; if it is set too low, it will cause the simulation to show throw (projection of discharge jet) as longer than in reality. Note that the velocity distribution along the length of the discharge slots is assumed to be uniform, which may not be realistic but is sufficient for the purposes of this simulation. Setting the appropriate discharge air temperature of the chilled beam requires some additional arithmetic to be implemented in the boundary condition. By applying a simple energy balance to the chilled beam, an equation for the discharge temperature T_m can be derived as a function of the preceding performance metrics:

$$T_m = \frac{T_p + K_{in} T_{in} + \frac{Q_{coil}}{\bar{\rho} C_p}}{1 + K_{in}} \quad (1)$$

where T_{in} is the temperature of the induced air, which is calculated by the simulation from the induction opening boundary. The sign convention for coil capacity is a negative value in cooling and a positive value in heating. Because the specific heat capacity of air varies very little between 55 and 80°F, it can be taken at standard conditions. Air density, however, should be taken as an average between the induced air and primary air temperature. It is also assumed that the cooling capacity of the coil is fixed when, in reality, it is a function of the water flow rate and the temperature difference between the water and the induced air (as well as the primary airflow rate). Depending on how much information is available from the manufacturer, this dependence can be incorporated into [Equation \(1\)](#).

Solver and Models

A RANS approach is used with a finite-volume, fully coupled solver. The shear stress transport (SST) turbulence model is used to capture thermal effects near the walls with good accuracy for the velocity field as well (Zhang et al. 2011). A Monte Carlo model is used to capture the thermal radiation heat transfer in the space from all the heat sources. The buoyant force is computed directly from the density field and is important for modeling the cold downdraft from the windows, as well as accurately capturing the nonisothermal throw of the chilled beams.

Convergence

Convergence is judged by a combination of the normalized RMS residuals of mass and momentum, as well as the global energy balance in the domain. A solution is considered converged when the mass and momentum residuals fall below 1×10^{-4} and the global energy imbalance is less than 5%. The global energy imbalance (total energy coming in versus going out of domain) is a very important convergence parameter, and adding the mixed flow temperature equation generally tends to slow down convergence. The criterion of 1×10^{-4} for the normalized residuals is a frequently used rule of thumb that gives good convergence and sufficient accuracy for the purposes of this simulation. The 5% criterion for the global energy balance is based on experience and is a compromise between solution accuracy and the ability to converge the solution to a smaller tolerance.

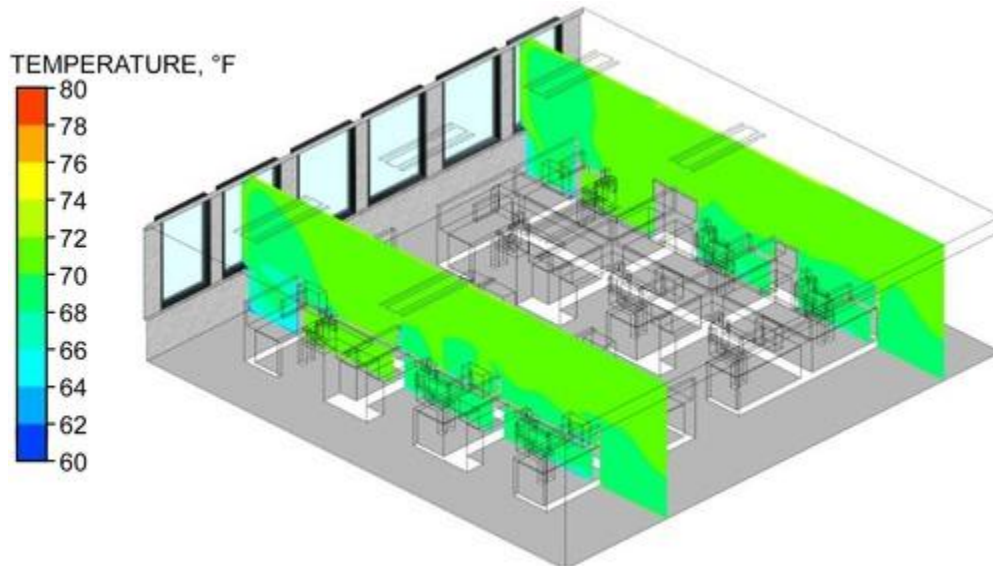


Figure 7. Vertical Temperature Contour Showing Cold Downdraft near Windows

Post Processing and Results

Figures 7 to 10 show results for one of the configurations in the example. Contour plots of temperature, velocity, predicted mean vote (PMV), and contaminant removal effectiveness are shown. PMV is a thermal comfort metric that correlates the thermal comfort response of a large group of occupants to various flow field variables such as velocity, temperature, humidity, and thermal radiation, as well as occupant properties (e.g., clothing insulation, activity level). This metric is based on the seven-point comfort scale described in detail in ASHRAE *Standard* 55. The band between 0.5 and -0.5 on the PMV scale is considered to be acceptable. Contaminant removal effectiveness is defined as a ratio of contaminant concentrations (see Chapter 15 of Zhang [2004]) from a chosen surrogate tracer gas. It is one way of measuring how efficiently the HVAC system distributes the ventilation air; for other approaches, see Etheridge and Sandberg (1996).

The results show some nonuniformities in the space temperatures, with a noticeable cold zone near the window, most likely caused by the downdraft of cold air. The thermal comfort varies throughout the space as well, with a cold zone near the windows due to the downdraft. The streamline plot shows that the chilled beams do a good job of washing the windows, as well as the collision zone above the occupants. The contaminant removal effectiveness (CRE) is reasonable, although some stagnant zones ($CRE < 1$) are evident in the back cubicles.

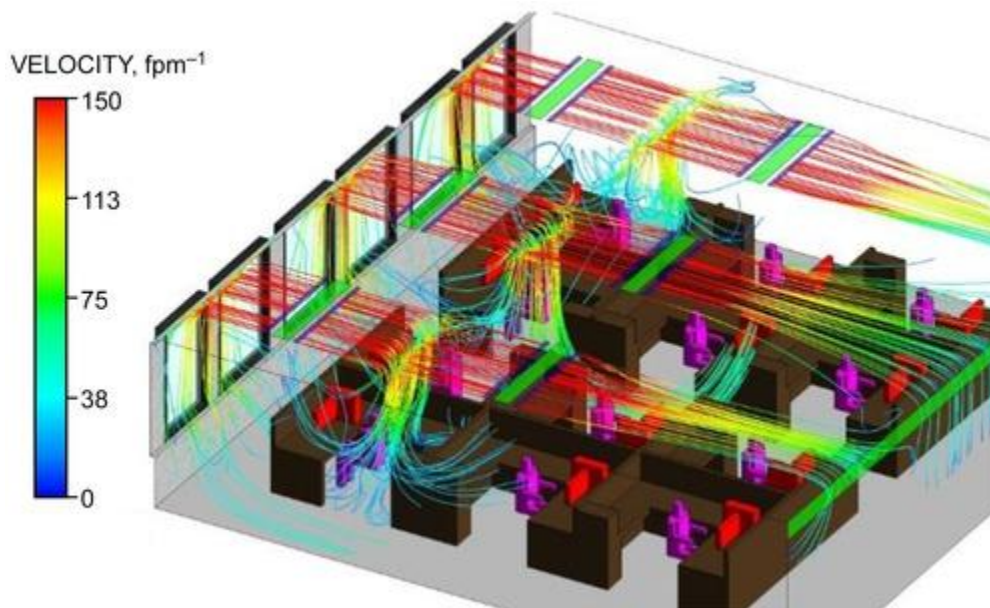


Figure 8. Velocity Streamlines Showing Supply Air Velocity and Direction

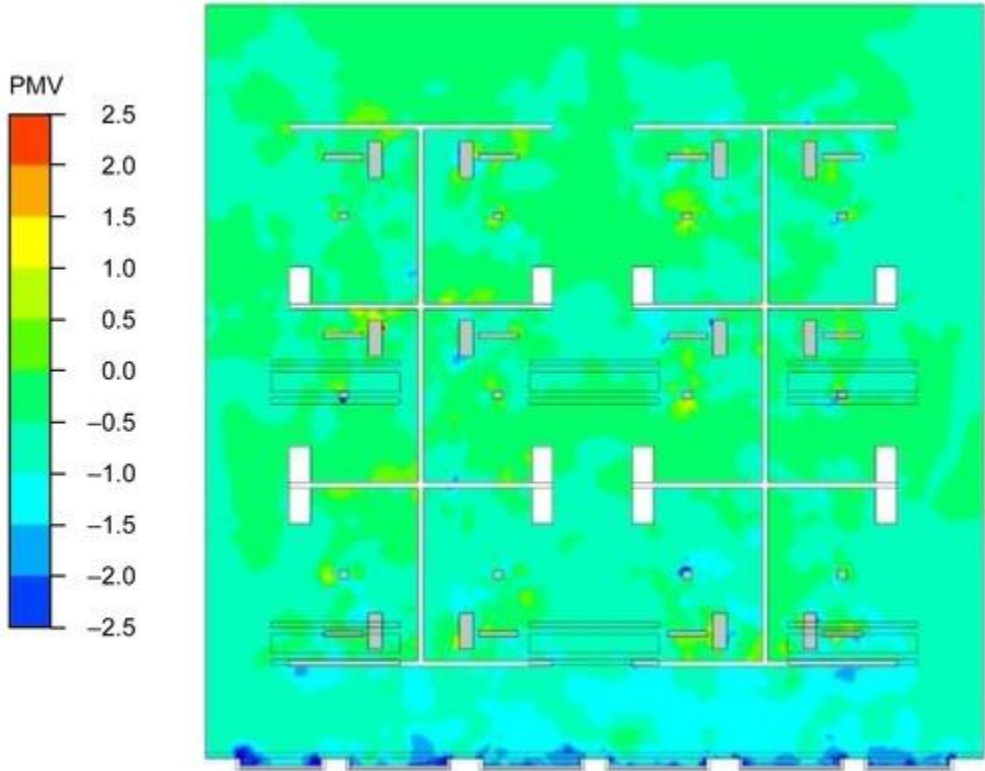


Figure 9. PMV Contour Plot 42 in. Above Floor

3.3 DISPLACEMENT VENTILATION

In some cases, displacement ventilation (DV) might be more appropriate than the common mixing HVAC solution. However, with the lack of mixing, controlling air stratification in the indoor environment becomes crucial. The purpose of this CFD example is to investigate the performance of a displacement ventilation system by analyzing the thermal comfort, stratification, and ventilation effectiveness in the space.

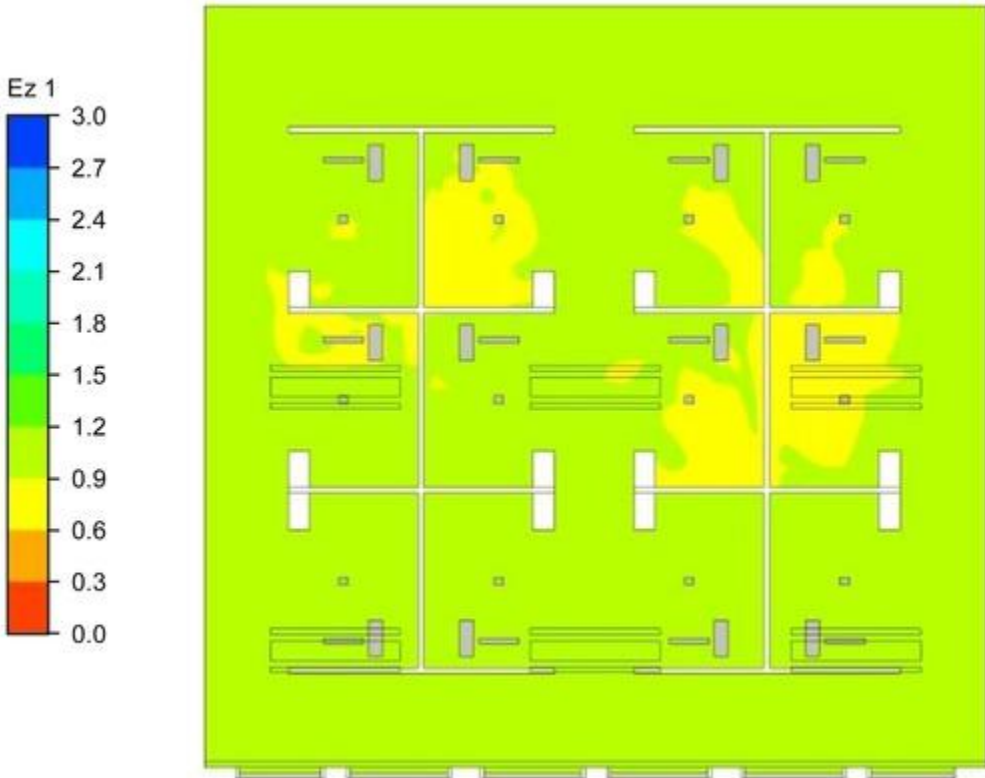


Figure 10. Contaminant Removal Effectiveness (CRE) 42 in. Above Floor (Seated Breathing Height)

Model Geometry

The classroom is an 861 ft² space with a 10 ft high ceiling, an exterior window, and a radiant slab with two controlled zones (interior and exterior). The classroom has a projector and a teacher's desk, as well as other furniture, including multiple cabinets and tables. The classroom is conditioned with three wall displacement diffusers on the side walls and two returns located on the ceiling near the exterior window. The various modeling decisions made for this specific case follow. [Figure 11](#) shows a simplified representation of the gross geometry of the classroom. The geometric features in this CFD model are

- Furniture (e.g., tables and wall cabinets)
- Simplified occupants (seated students and a standing teacher)
- Projector
- Exterior window (surface, no mullions)
- Displacement diffusers (inlet)
- Returns in the ceiling (outlet)

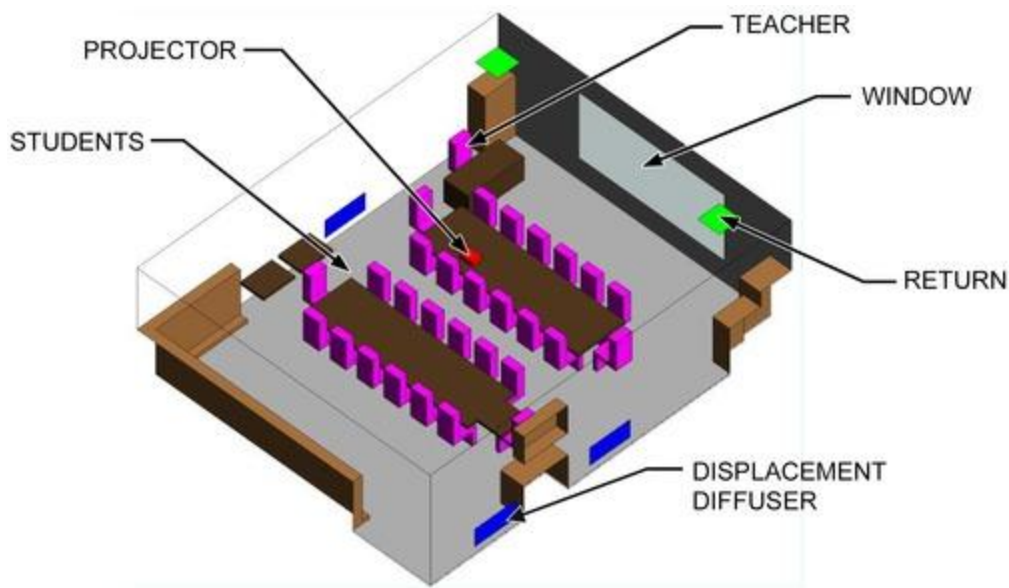


Figure 11. Classroom CFD Model: Simplified Geometric Model

The spaces under the tables are included in the model because airflow moves along the floor in a displacement system. It is therefore important to avoid flow obstructions that do not exist in the real space. In addition, the surface of the table affects the dynamics of the thermal plumes of the seated occupants. There are 35 occupants, so simplified models are used to represent them. They are meant to capture the rough geometric shape of a seated occupant while retaining the total surface area of an average-sized seated adult male (see [Chapter 9 of the 2021 ASHRAE Handbook—Fundamentals](#)). It is acknowledged that there is some loss in accuracy, because the occupants are actually children. The standing teacher is modeled as a simple rectangular prism, with the appropriate surface area.

Mesh Generation

A snapshot of the computational mesh in a horizontal and vertical plane is shown in [Figure 12](#). A tetrahedral mesh is used in this example; it can efficiently handle complex geometries and is less sensitive to random changes in flow direction like the hexahedral mesh. This is particularly important in displacement flows where thermal plumes (direction not known a priori) dominate the flow. It is also less labor intensive to generate for the geometry used in this example. Local mesh refinement is used around the various geometric features, with particular attention paid to local refinement around the heat sources (to capture thermal plumes), the displacement diffuser (to capture the three-dimensional floor jet), and, to a lesser extent, the returns. Mesh refinement perpendicular to all the surfaces in the model is used to capture the thermal and hydrodynamic boundary layers. For the current turbulence model, 12 layers of prismatic elements are used at the walls with a dimensionless wall distance of $y^+ < 2$ for the first layer. In this simulation, a global mesh size of 9 in. is used, and mesh sizing of 2.5 in. and 2 in. is used around the return and the occupants, respectively. A mesh size of 1 in. is used on the displacement diffuser to capture its waterfall flow pattern as well as the complex three-dimensional thermal wall jet. Refinement around a displacement diffuser is typically coarser than a mixing diffuser at the same flow rate, as a result of the shorter projection distance and the velocity of the jet. A mesh

growth ratio of 1:15 is used around the displacement diffusers, the occupants, and the projector, to ensure that this mesh refinement smoothly merges into the larger cell size of the room.

Boundary Conditions

The boundary conditions for this example are

- **Returns:** No relative pressure, temperature, scalars, and turbulence quantities are extrapolated from the solution (do not need to be specified).
- **Window:** Specified with a convective heat flux to model heat conduction through the glass, and a directional radiant heat flux to model the solar heat gain. The direction is based on the position of the sun at the time the peak load occurs, and can be calculated using [Chapter 15 of the 2021 ASHRAE Handbook—Fundamentals](#)
- **Occupants:** specified with radiant and convective heat flux, with 60% of the total heat gain being radiant and 40% being convective (see Table 1 in [Chapter 18 of the 2021 ASHRAE Handbook—Fundamentals](#)).
- **Lights:** specified with radiant and convective heat flux (80/20% radiant/convective split) ([Chapter 18 of the 2021 ASHRAE Handbook—Fundamentals](#)). Boundary condition applied to entire ceiling.
- **Projector:** specified with a radiant and a convective heat flux, with 15% of the total heat gain being radiant and 85% being convective (see Tables 8 and 11 in [Chapter 18 of the 2021 ASHRAE Handbook—Fundamentals](#)).
- **Radiant slab:** beyond the scope of this example.

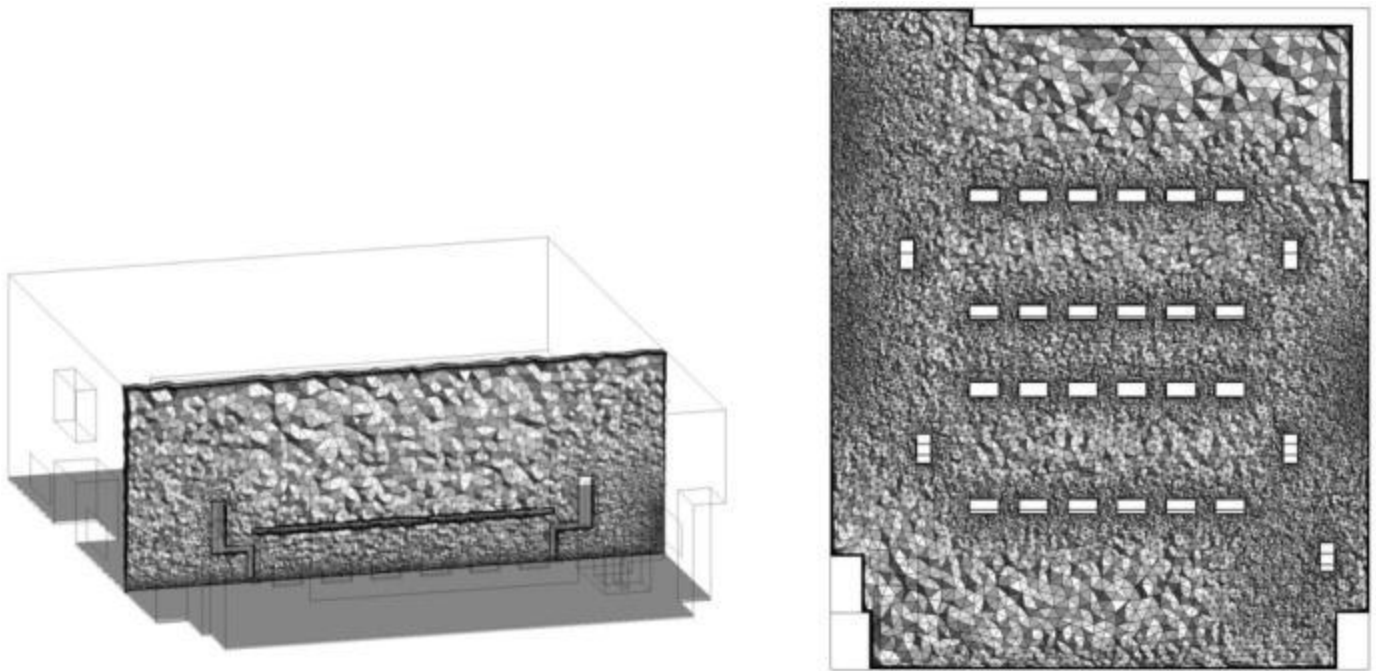


Figure 12. Classroom CFD Model: Computational Mesh Resolution at Vertical and Horizontal Plane

All radiation heat fluxes apart from the window are assumed to be isotropic (independent of direction). The displacement diffuser model is worth discussing in more detail. Although the face velocity of the diffuser is low and flow in the space is driven by the heat sources, it is important to accurately capture the velocity temperature distribution in front of the diffuser for an accurate assessment of thermal comfort. The model used in this example is a simplified version of the momentum method (Chen et al. 1999) that does not take the perforated face into account. In situ measurements have shown this to be a reasonable approximation for this type of diffuser. Note that better accuracy can be achieved with a more refined model.

Solver and Models

A RANS approach is used with a finite volume, fully coupled solver. The shear stress transport (SST) turbulence model is used to capture thermal effects near the walls with good accuracy for the velocity field as well (Zhang et al. 2011). A Monte Carlo model is used to capture the thermal radiation heat transfer in the space both from the short-wave (solar) and long-wave (e.g., people, lights) heat sources. Thermal radiation heat transfer from the ceiling to the cool floor also has a strong effect on the vertical temperature gradient in the space. The buoyant force is computed

directly from the density field and is a crucial component of the simulation, because the dynamics of displacement ventilation systems are driven primarily by buoyancy.

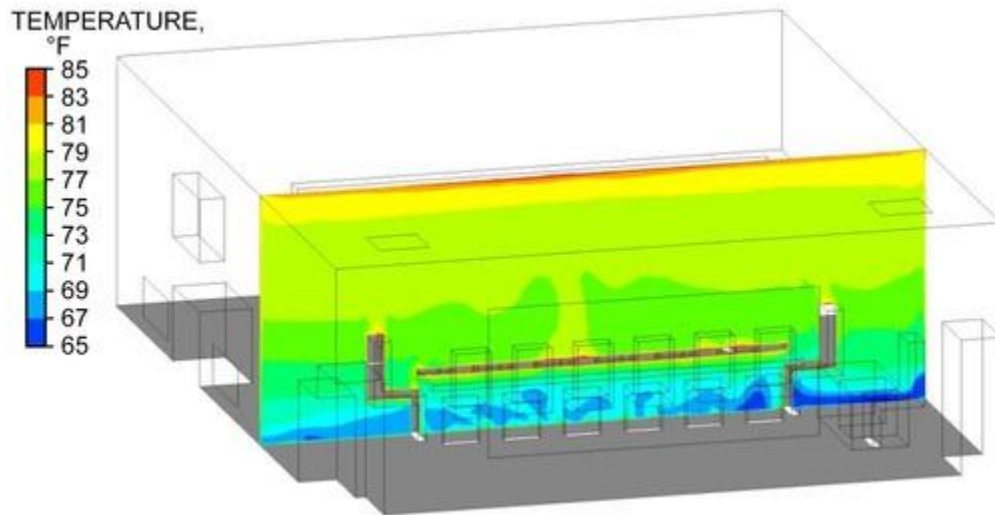


Figure 13. Vertical Temperature Contour Showing Stratified Temperature Distribution Typical of DV Systems

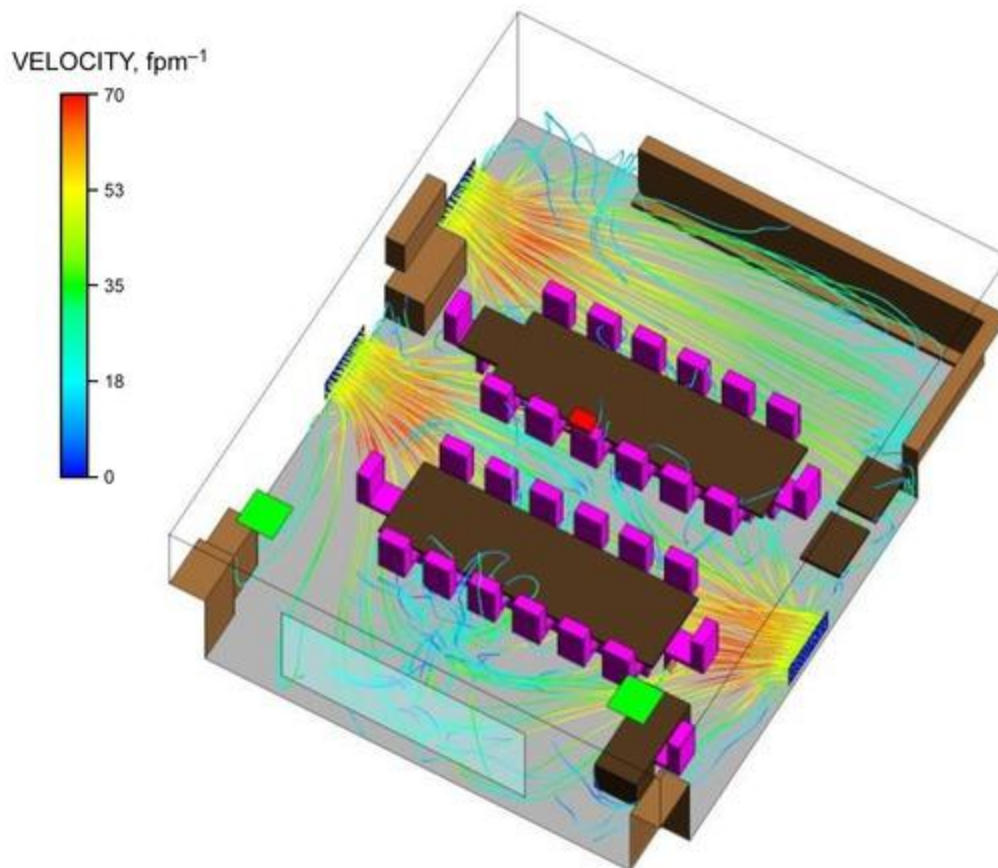


Figure 14. Velocity Streamlines Showing Supply Air Velocity and Direction

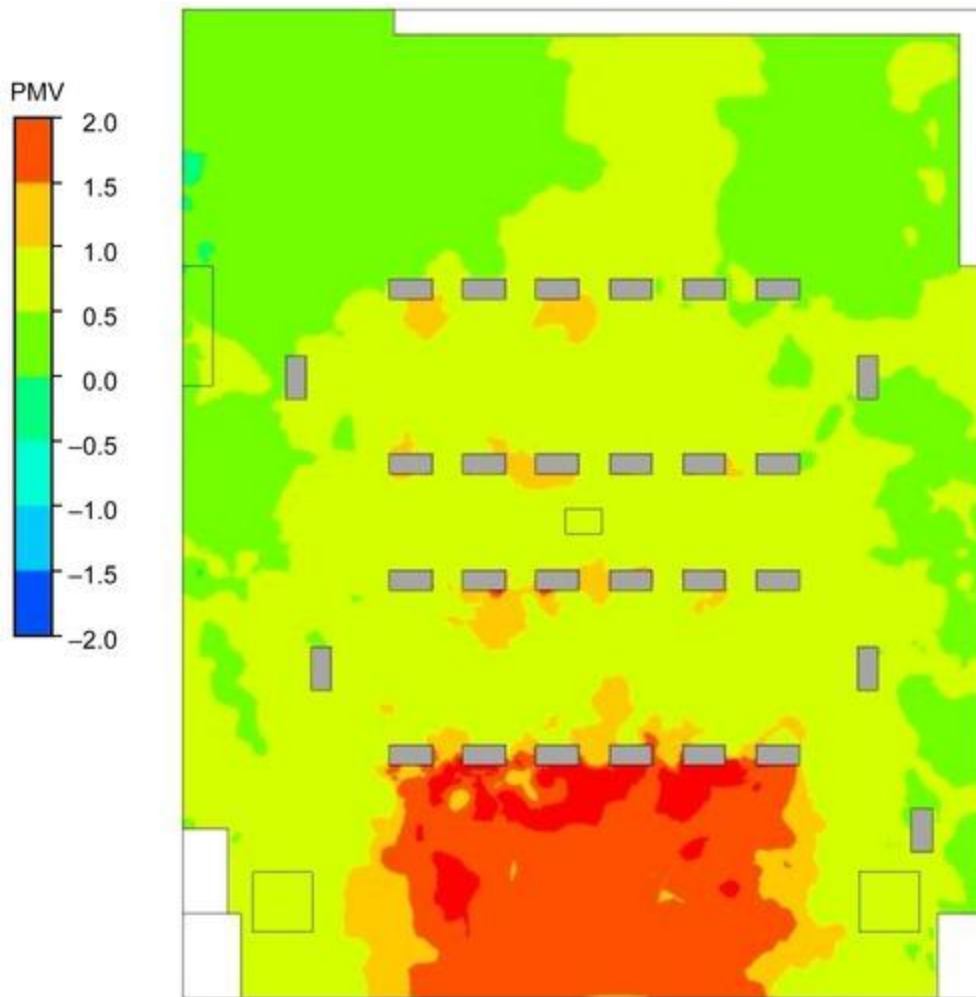


Figure 15. PMV Contour Plot 42 in. Above Floor

Convergence

Convergence is judged by a combination of the normalized RMS residuals of mass and momentum as well as the global energy balance in the domain. A solution is considered converged when the mass and momentum residuals fall below 1×10^{-4} and the global energy imbalance is less than 5%. The criterion of 1×10^{-4} for the normalized residuals is a frequently used rule of thumb and gives good convergence and sufficient accuracy for the purposes of this simulation. The global energy imbalance (total energy coming in versus going out of domain) is a very important convergence parameter for displacement ventilation problems, because the thermal field takes much longer to stabilize than the hydrodynamic field. For example, the mass and momentum equation residuals can stabilize and converge before the global energy balance reaches its converged state, which yields the wrong solution (no thermal stratification).

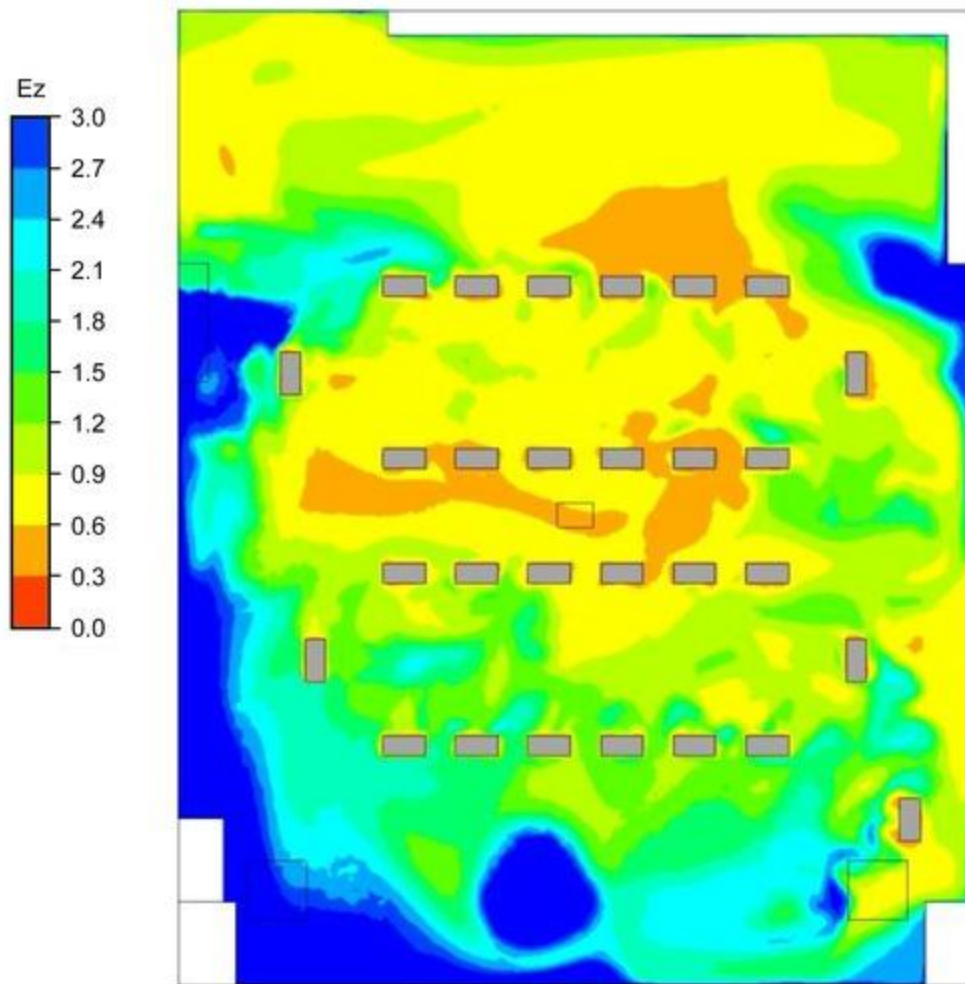


Figure 16. Contaminant Removal Effectiveness (CRE) 42 in. Above Floor (Seated Breathing Height)

Post Processing and Results

Figures 13 to 16 show results for one of the configurations investigated in the study. Contour plots of temperature, velocity, predicted mean vote (PMV), and contaminant removal effectiveness are shown. The contaminant removal effectiveness is defined as a ratio of contaminant concentrations (Zhang 2004) from a chosen surrogate tracer gas. It is one way of measuring how efficiently the HVAC system distributes the ventilation air. The results show good thermal stratification in the space with a layer of cold air spread across the floor. The streamline plots imply that the specific arrangement of diffusers does a good job distributing the cool supply air across the floor and around all of the flow obstructions in the space. The PMV plot shows a very distinct hot spot under the window, which is a direct consequence of the magnitude and direction (pointed down) of the solar load. Overall, the thermal comfort in the space is slightly outside the desired comfort range (on the warm side). Contaminant removal effectiveness is also not very uniform, suggesting that some improvements can be made to the air distribution system to better distribute the supply air.

3.4 DATA CENTER DESIGN

Due to the intense cooling load of the computers (compared to human occupants), modeling of data centers is a drastically different challenge for HVAC design (ASHRAE *Standard* 90.4). The following example demonstrates use of CFD in design of this unique type of facility.

This example involves a 7400 ft² raised floor data center containing 138 information technology (IT) racks and 192 perforated floor tiles, as shown in Figure 17. The IT racks are arranged in rows, forming five cold aisles and four hot aisles. Twelve floor-mounted power distribution units are located along two opposing sides of the room. The IT and power distribution equipment collectively consume over one million Btu/h of power, and the floor tiles supply 102,528 cfm of air to the room, at an average airflow rate of 534 cfm. Warm air returns to the cooling system through perforated ceiling tiles located above the hot aisles, which feed into a large open ceiling plenum. CFD is useful both to aid in the design of data centers and to optimize the performance of existing facilities (Healey et al. 2014; VanGilder and Seymour 2014); this example focuses on the latter.

Geometry Generation

In contrast with many general-purpose CFD tools, which require the user to assemble models using simple geometric primitives, data-center-specific CFD modeling tools and electronics-specific modeling tools typically provide high-level building-block objects that only need to be configured to represent the geometry and operating conditions of a given data center. For example, racks, coolers, or tiles can be selected from a library of objects and simply placed into the room.

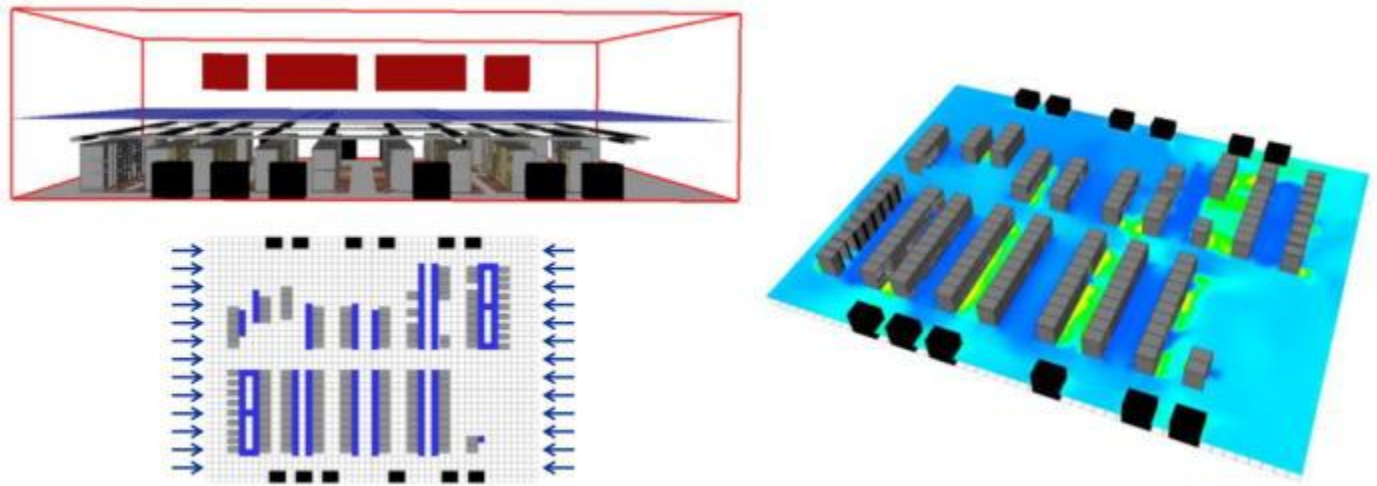


Figure 17. Data Center Layout

To best capture the physics that govern a given data center's airflow patterns, it is recommended that the floor plenum be modeled together with the whitespace. However, it may be simpler to model the two spaces separately, and in cases where the floor tiles are fairly restrictive (in the range of 25% open area or less), doing so delivers reasonable accuracy.

Mesh Generation

The example data center was modeled using a rectangular Cartesian grid, which maps well to typical data center geometry. Generally, cells of side length 6 in. or smaller are recommended (Zhang 2008) for modeling data centers. In the example case, grid cells in the whitespace were set to have a maximum side length of 6 in. and a minimum side length of 1 in. below the dropped ceiling. The variation in grid cell dimensions allows for finer grid cells near objects and complex geometry, and larger grid cells in open space. However, the model uses grid cells of up to 24 in. on a side within the ceiling plenum, which is largely open space and far away from features of interest.

Solver and Models

The example case uses a RANS CFD solution methodology, assuming steady-state conditions, and the standard k - ϵ turbulence model was employed.

Boundary Conditions/Object Modeling

Several specific modeling choices resulted in greater accuracy of the example model. Because the room is located inside a larger indoor enclosure and there is little heat transfer across the room walls, walls were modeled as adiabatic solid boundaries. Additionally, rather than modeling each rack as a monolithic box with uniform airflow into the front face and out of the rear (as per Zhai et al. [2012]), each rack was subdivided into a number of slices (Pardey et al. 2015), as shown in [Figure 18](#). Each slice was assigned its own airflow rate and accordant temperature increase based on its power, with the assumption that servers draw 0.04 cfm per Btu/h. Blanking panels were modeled as solid blocks, and open spaces were modeled as open. Rack doors were modeled as two-dimensional flow resistances coincident upon the front plane of the rack. A vertical momentum source was enforced inside a volume region over each tile extending to a height of 4 in., in the method of Abdelmaksoud et al. (2010), to accurately model the jet-like tile airflow. Inside the floor plenum, care was taken to explicitly model the vertical stanchions that support the raised floor. However, stanchions can equally be modeled as a distributed resistance, as discussed in VanGilder et al. (2016).

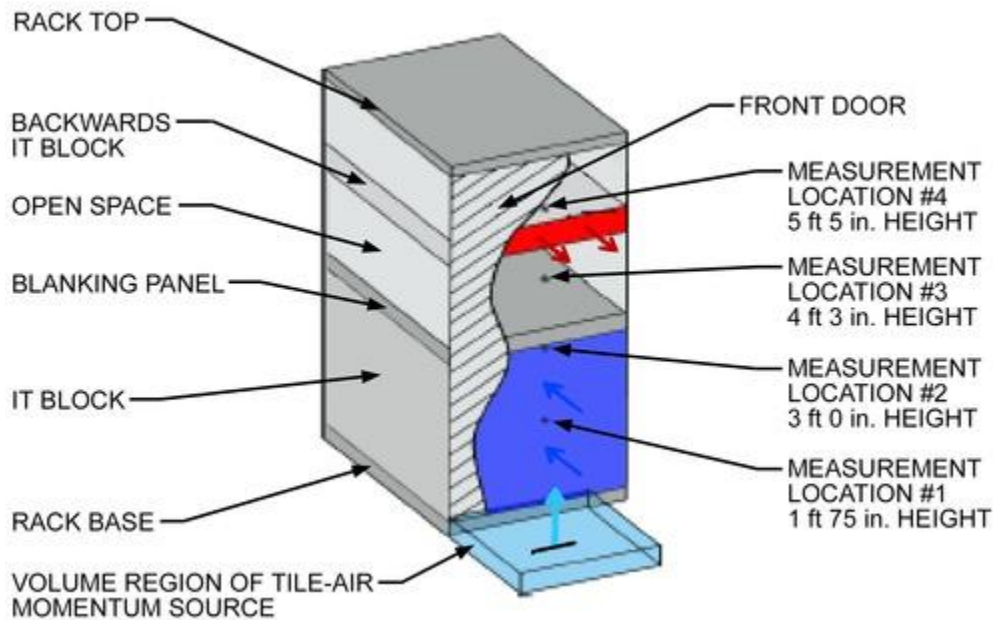


Figure 18. Rack Model

Individual perforated floor tile airflow rates were measured using the anemometer scaling method described in VanGilder et al. (2016). The floor of the example facility is bolted and gasketed, preventing any significant air leakage, so the sum of floor tile airflows was considered to represent the total room airflow. To simulate airflow patterns inside the floor plenum, the total room airflow was divided among the 21 airflow inlet bays that feed the plenum, and each bay was modeled as a fixed-flow boundary condition. The portion of the total room airflow allocated to each bay was calculated based on measured air velocity through each given bay. It is important to note that total room airflow could also be estimated by summing the nameplate flow rates of all active computer room air-handler (CRAH) units, or by measuring airflow from CRAHs using an anemometer or a flow hood.

Convergence/Grid Independence

The model is considered converged when residual errors in the mass, momentum, energy, and turbulence-model equations reach a predefined level, which is usually set to a default value. Here, in accordance with best practices, a number of simulations were performed using computational grids with varying cell sizes. By comparing the predicted temperatures and airflow patterns produced by simulations with different cell sizes, grid independence was established.

Model Calibration

The CFD model was created to help optimize performance of an existing data center, so greater detail was required than would be necessary for preliminary design purposes. As such, the model was calibrated by iteratively increasing the detail and fidelity of its construction based on measurements and observations. Key parameters for accuracy were inlet rack temperature and tile airflow rate. Rack inlet temperatures were measured at four equally spaced points along a vertical line at the center of the face of each rack.

The accuracy of the model was enhanced by dividing each rack into 42 individual one-unit slices, each of which was either occupied by an active piece of IT equipment or blanking panel or was left open. Additionally, because IT equipment often generates jets of warm exhaust air, it was important to account for any IT equipment that produced such jets directed into a given cold aisle (either inadvertently or because of suboptimal equipment design). Including the doors of racks in the model as two-dimensional flow resistances also improved accuracy. In the floor plenum, accuracy was increased by modeling the vertical support stanchions, because it was discovered that if the stanchions were not included in the CFD model of the plenum, the model produced substantially different tile airflow predictions.

Capturing accurate input data is equally as important as making appropriate modeling choices, and to this end, it was crucial to account for the resistance of the flow hood on the measured perforated tile airflow rates. Methods for doing so have been evaluated at length in Zhang (2004). Note that CRAH return temperatures to the cooling system could also be used as a criterion by which to evaluate the accuracy of the CFD simulation or check the consistency of other assumptions.

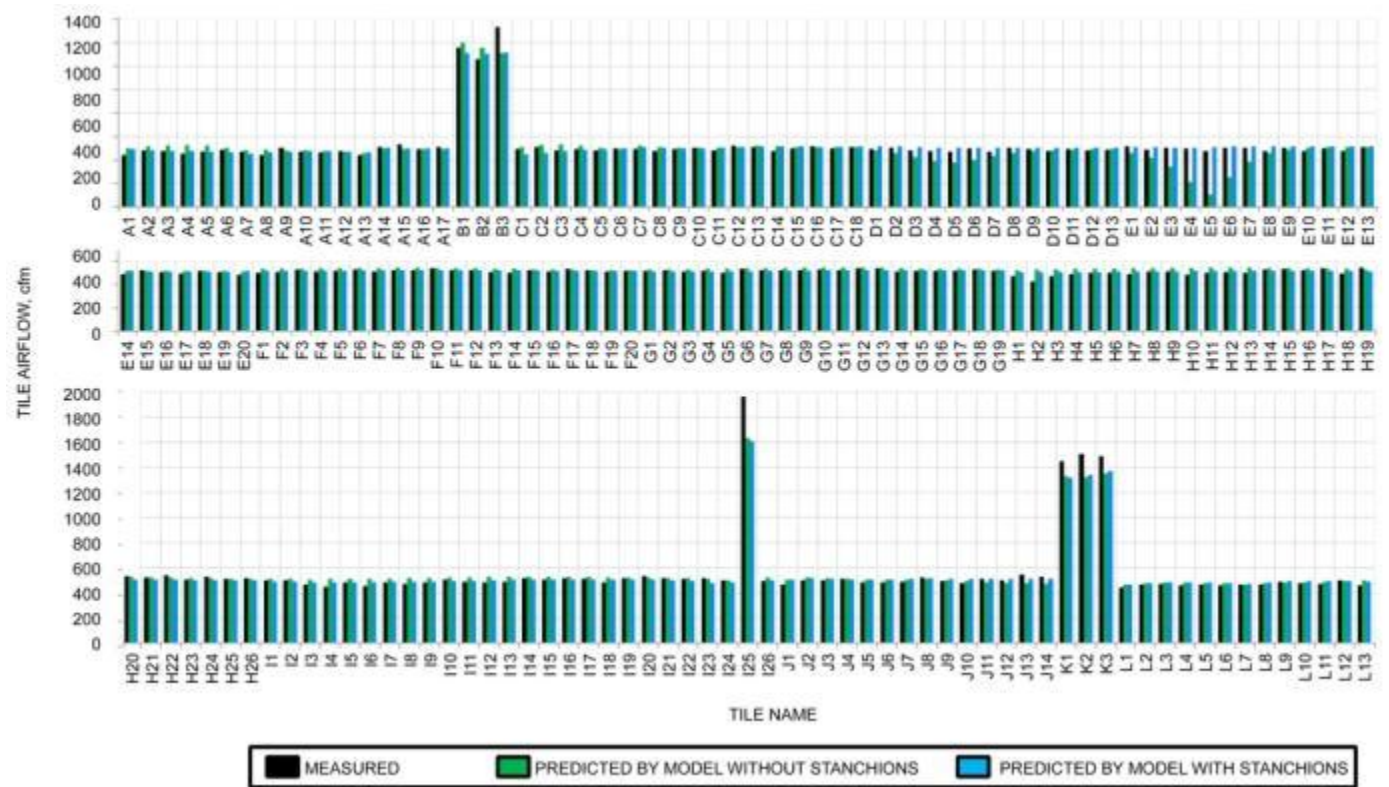


Figure 19. Comparison of Measured and Predicted Tile Airflow Rates



Figure 20. Comparison of Measured and Predicted Rack Inlet Temperatures

Results

The model was created specifically for managing and optimizing an existing data center. Therefore, it was necessary to model in more detail than is required for preliminary design purposes. [Figures 19](#) and [20](#) show the results of predicted versus measured perforated tile airflows and rack inlet temperatures, respectively. [Figure 19](#) shows two variants of the plenum simulation: one that includes raised-floor support stanchions and one that does not. The model that includes stanchions predicts 186 of 192 tiles to within $\pm 10\%$ of the individual measured airflows and the remaining six tiles to within $\pm 20\%$. [Figure 20](#) depicts predicted rack inlet temperatures according to their accuracy and shows that the calibrated model predicts 105 of the 115 active racks with an error rate of less than 10% of the maximum temperature range observed in the data center. To achieve this level of accuracy, it was important to model the contents of each rack at the unit (U) level, rack doors as flow resistances, momentum sources above each perforated

Additional Resources

A recent ASHRAE research project (RP-1675; Lin 2022) establishes guidelines for data center CFD modeling. In addition to providing general background information, the report provides information particularly useful to users of general-purpose CFD and developers of data-center-specific CFD tools. The project conducted a comprehensive literature survey and concluded that best-practice modeling techniques for data centers continue to evolve and that the modeling community requires clear guidelines particularly for modeling common data center equipment such as IT racks, cooling units, and perforated tiles. Such guidelines support the use of CFD modeling for design and operation applications and lead to more reliable and energy-efficient data centers. To support the development of guidelines, CFD simulations were validated by experimental measurements in a small lab-scale data center that featured a traditional raised-floor plenum for distributing cooling airflow to perforated floor tiles and, ultimately, to the IT equipment (IT simulators in the study) housed in racks. The guidelines therefore focused on modeling underfloor-vertical-axis blowers and perforated tiles which were present in the test data center.

Based on this work, it is recommended that compact blower models include explicit representations of the blower shape and location and account for both normal and tangential velocity components. Compact perforated tile models should include the correct pressure drop characteristics (for which good estimates are not always easy to obtain), airflow straightening (to remove tangential velocity components), and a downstream momentum source (to compensate for momentum lost when assuming airflow is spread uniformly over an entire tile face). Based on the literature review and CFD-based sensitivity studies performed in the study, general advice is also provided for other common data center features. Interested readers are encouraged to review the RP-1675 final report, which is available from the ASHRAE Technology Portal (technologyportal.ashrae.org; free to ASHRAE members).

3.5 VIRAL CONTAINMENT IN HOSPITAL WARD

The goal of air distribution inside a hospital operating room (OR) is to protect the patient and staff from cross infection while maintaining occupant comfort and avoiding impediment of surgical tasks. In ORs, HEPA-filtered air and vertical (downward) laminar airflow are often used to achieve a unidirectional flow of fresh air from the ceiling, washing over the patient and flowing out of exhaust vents on the side walls, near the floor.

A CFD tool was used to predict the flow pattern and contaminant transport in a representative OR environment with standard airflow settings. The CFD model was first developed by Zhai et al. (2013) and validated against the full scale laboratory experiment; this example uses Zhai et al.'s diffuser specifications and air changes per hour (ach), as well as the same room, equipment, and occupant conditions (Table 1 and Figure 21). The equipment thermal loads (heat flux), as well as the temperature of the patient's wound and skin, can be seen in Table 2. Table 3 indicates the sizes of all of the objects in the room. These parameters provided crucial inputs for the following CFD model process.

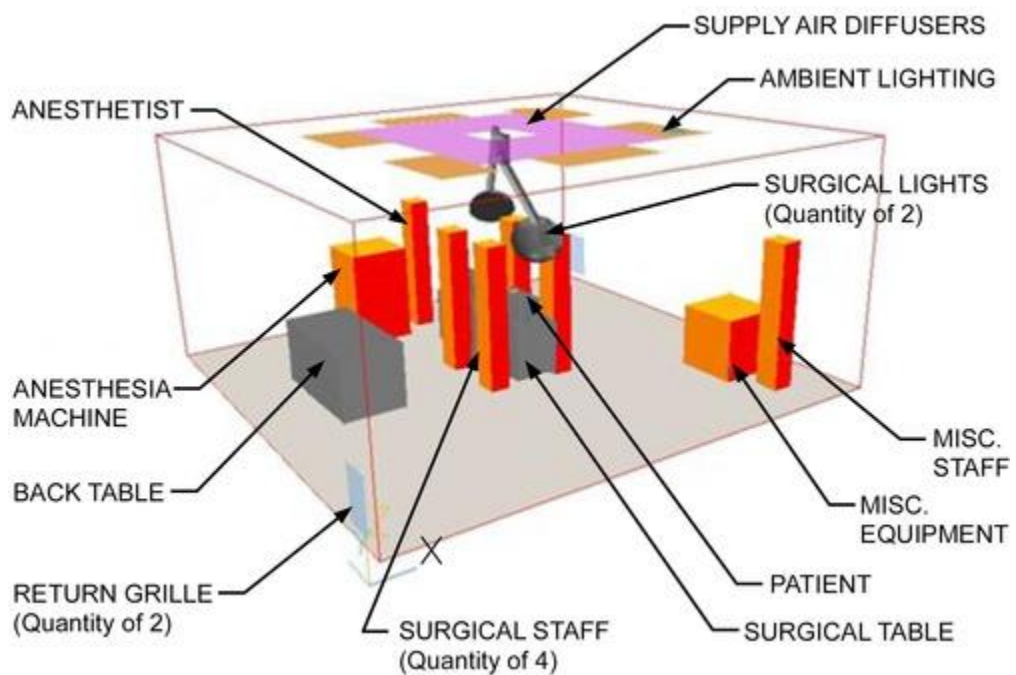


Figure 21. Base CFD Model Setup

Table 1 Laboratory Experiment Specifications

Room dimensions	20 × 19 × 9.5 ft
Diffuser dimensions	8.01 × 10.01 ft
Diffuser coverage area	76 ft ²
Air change rate	31.6 ach
Nominal face velocity	24.99 cfm/ft ²
Room air temperature	68°F
Supply air temperature	64.9°F
Room pressurization	+0.01 in. of water

Table 2 Laboratory Thermal Boundaries

Object	Qty	Heat Gain Btu/h	Temperature °F
Manikins, male	2	273 Btu/h	N/A
female	4	232 Btu/h	N/A
Anesthesia machine	1	341 Btu/h	N/A
Surgical lights	2	853 Btu/h	N/A
Monitor	1	682 Btu/h	N/A
Ambient lights	6	437 Btu/h	N/A
Patient wound	1	N/A	78.1
Patient skin	2	N/A	81.3

Geometry Generation

Melikov and Kaczmarczyk (2007) discuss the importance of detailed indoor objects such as a human body on indoor airflow characteristics, and indicate the local impacts of most details of indoor objects. Focusing on the general indoor airflow patterns and interactions between patient and medical staff, they simplified the simulation of indoor subjects such as human bodies and equipment (except for surgical lighting) as rectangular geometries with exact heat sources as tested. This practice facilitates the generation of high-quality meshes and therefore improves both speed and accuracy of the simulations.

Table 3 Room Object Dimensions

Object	Qty	Dimensions ft
Surgical table	1	1.77 × 6.17 × 2.17
Back table	1	2.49 × 4.99 × 2.49
Anesthesia machine	1	2.49 × 2.49 × 3.94
Surgical lighting	2	1.9 diameter
Misc. equipment (monitor)	1	2.49 × 2.49 × 2.49
Surgical staff	6	0.82 × 0.98 × 5.74
Patient body	1	0.98 × 5.25 × 0.82

Mesh Generation

A rectangular Cartesian grid, which maps well to typical OR geometry, was used. Local grid refinement was implemented near critical spaces and objects such as walls, inlets, and persons. The results of a CFD simulation are highly dependent on the quality of the computational grid. The grid refinement study was conducted on the following grids: 70 × 58 × 45 (180 k cells), 87 × 73 × 57 (362 k cells), 106 × 91 × 70 (675 k cells), 124 × 111 × 86 (1.2 million cells), and 155 × 142 × 108 (2.4 million cells). [Figure 22](#) demonstrates the finest grid distribution.

Solver and Models

Both RANS and LES CFD methods were tested for this example case. Although advanced CFD modeling techniques such as LES provide substantial benefits, the currently available RANS technologies have proven to be adequate for modeling the steady-state characteristics of the hospital operating room air distribution. In the RANS CFD solution methodology, the RNG k - ϵ turbulence model (Yakhot and Orszag 1986) was used, as suggested by Zhang et al. (2007).

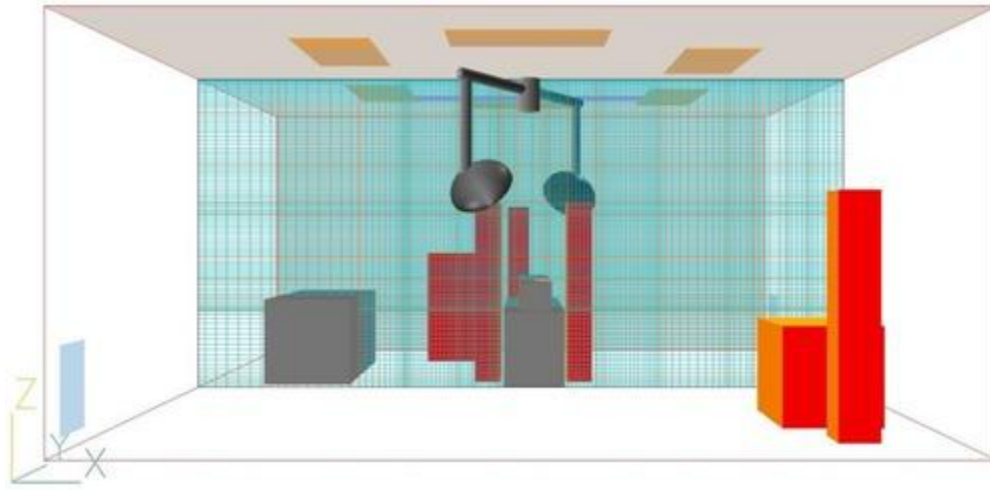


Figure 22. Grid Refinement Case: 7.8 ft Cells

Boundary Conditions/Object Modeling

Most indoor objects such as persons and equipment were specified straightforwardly using the standard wall/block boundary condition methods. Inlet boundary condition is critical to accurate CFD modeling of indoor environments, because this is the primary source of momentum responsible for overall room air distribution pattern. Srebric and Chen (2002) performed a comprehensive analysis of diffuser boundary conditions to determine appropriate simplified boundary conditions, and found the box and momentum methods to be the most appropriate for the diffusers that were tested. The momentum method was used in this example, based on the recommendation of Chen and Srebric (2012) for the grille diffuser that is similar to the nonaspirating diffuser type.

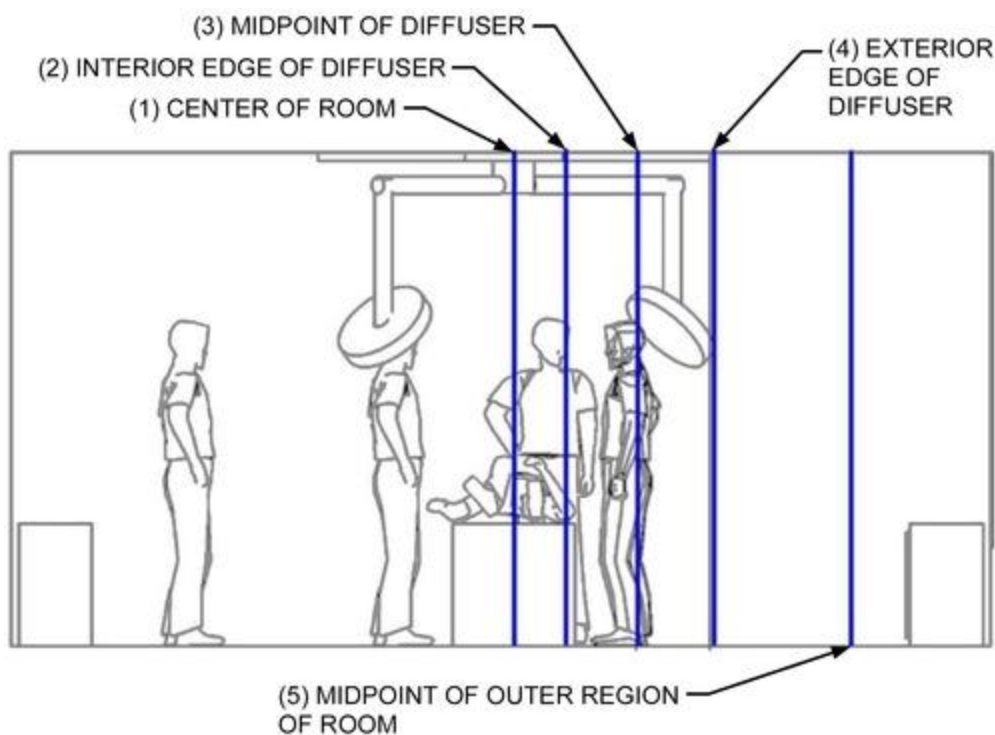


Figure 23. CFD Grid Refinement Measurement Locations in Central Cross-Sectional Plane

Convergence/Grid Independence

The simulation was considered converged when the sums of residual errors in the mass, momentum, energy, and turbulence-model equations reached a predefined level (0.1%). The grids of different sizes were evaluated using the normalized root mean squared error (NRMSE) of the CFD model results with different grids (Wang and Zhai 2012). [Figure 24](#) shows the NRMSE of the predicted x and y direction velocity at the four measure poles (1 to 4) across the center axis of the room, 9.45 ft high ([Figure 23](#)), between the 180k and 362k meshes and the 675k mesh. It reveals that there is generally a great improvement in error with the 362k mesh; the computational error is typically below 10%, and absolutely below 30%. Based on this, and to minimize the simulation time, the 362k mesh was chosen for various parametric simulations.

Model Validation

The simulation replicates the airflow pattern as observed in the lab (see Chapter 13 of the 2017 *ASHRAE Handbook—Fundamentals*): an inward curvature of the airflow to the center of the jet stream, as seen in [Figure 25](#). This behavior reduces the overall coverage area and could pose a contamination risk to the patient.

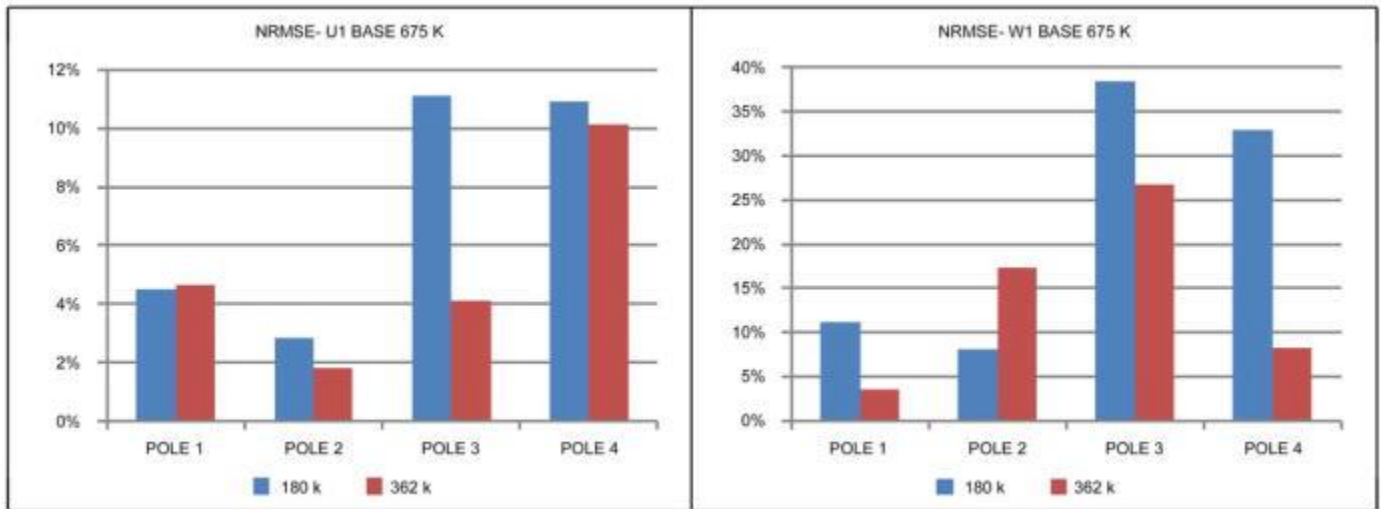


Figure 24. NRMSE Comparison Between 180k and 362k Meshes and 675k Mesh

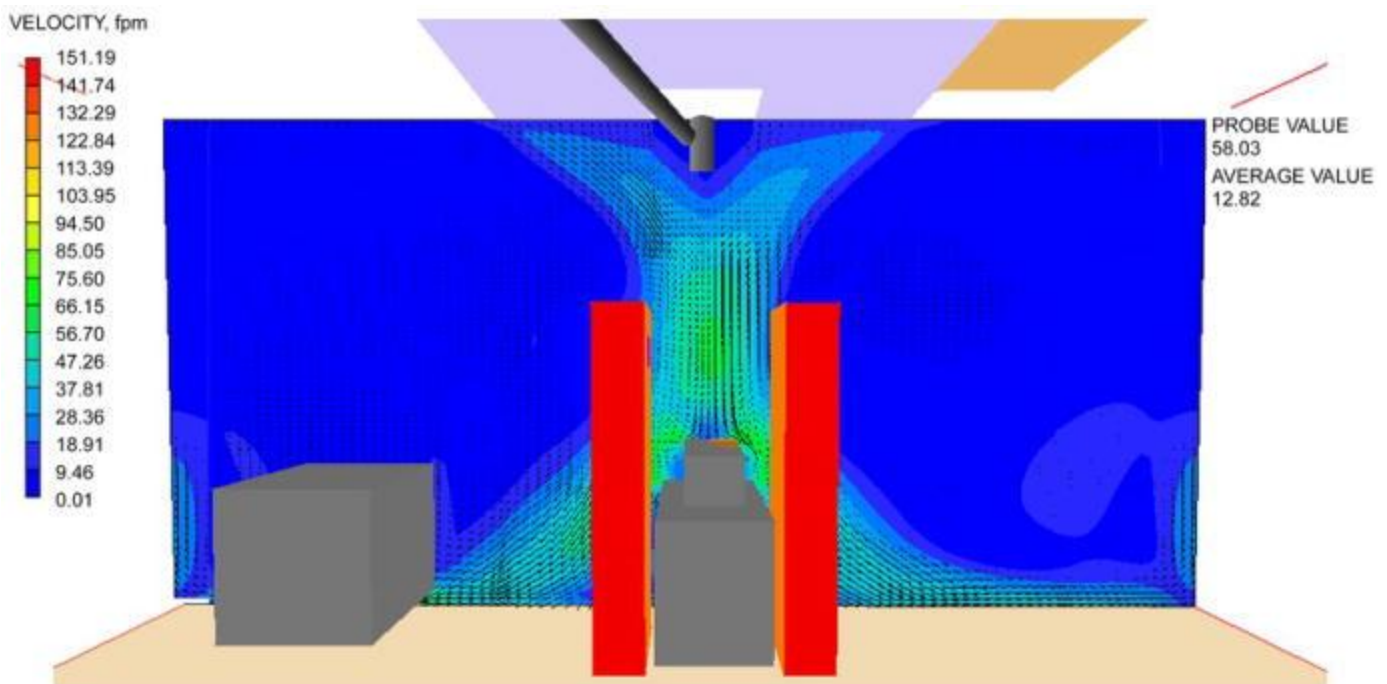


Figure 25. Velocity Vectors and Contours at Central Cross Section with 675k Grid

The quantitative comparisons of simulation and experimental results were plotted in [Figures 26](#) and [27](#), for x and y velocity components, respectively. [Figures 26](#) and [27](#) show that the CFD simulations closely follow the experimental results, with a few exceptions. It also appears that there is, in general, a large difference between the experimental results and the 180k mesh, but a smaller difference between each of the latter meshes.

Results

This example demonstrates the applicability of CFD for modeling and analysis of airflow in the surgical environment. Although CFD can be accurately used for modeling indoor air distribution and contaminant transport in operating rooms, the CFD user must be extremely careful in implementing these models, to ensure accurate simulation of airflow. The sensitivity of airflow to thermal characteristics of the indoor environment makes the model sensitive to heat gain input parameters. The heat gain and inlet boundary conditions must be carefully selected to ensure that the resulting air distribution patterns are correct.

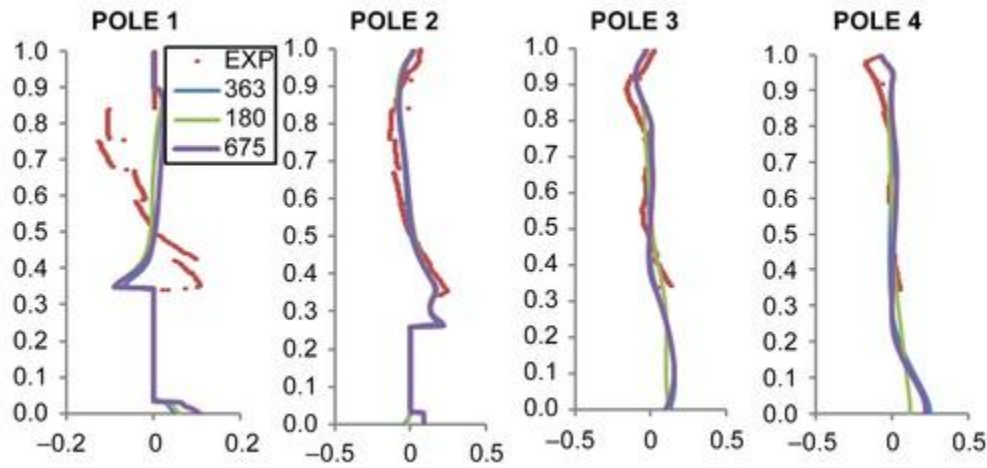


Figure 26. Comparison of U-Velocity in X Direction

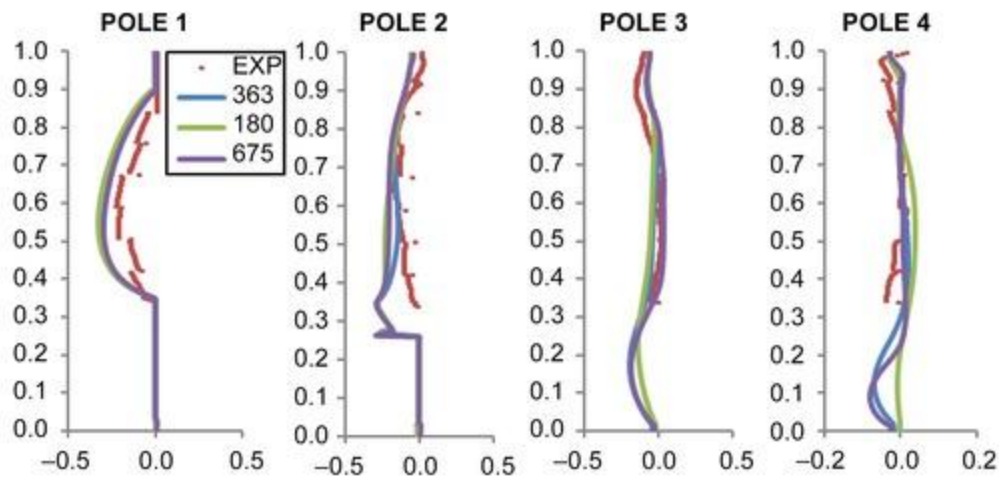


Figure 27. Comparison of W-Velocity in Z Direction

The following modeling methods were found to adequately model the represented physics identified in the operating room air distribution.

- Steady-state RANS
- RNG k - ϵ turbulence model
- Boussinesq approximation
- Hybrid differencing scheme
- Isothermal Lagrangian particle model

The general indoor environment conditions place the operating room indoor air distribution in the mixed convection category, but high cooling loads can lead to a strongly buoyancy-driven flow, verified by the parametric study of the Archimedes number of the supply air jet in the OR. The study reveals that the dependence of the room air distribution on the Archimedes number of supply air jets, rather than face velocity of supply diffuser, is of significant importance.

3.6 NATURAL VENTILATION

This example concerns a densely occupied, naturally ventilated auditorium, the key space at Lichfield Garrick, a performing and static arts center (Gorst 2003). This is one of several advanced naturally ventilated (ANV) buildings (Cook and Short 2005) that use low-energy design principles such as night cooling, thermal mass, buoyancy-driven stratification, and solar shading to enable natural ventilation to deliver thermal comfort in spaces with high heat gain. The Lichfield Garrick is comprised of foyer and bar areas surrounding a 500 seat auditorium and smaller studio space (Figure 28).

The large-volume space is ideally suited to buoyancy-driven natural ventilation, wherein the warm, stale air can be held above head height. The additional challenge in this space, however, was the presence of balcony areas, which meant careful concept design and computer modeling were required to ensure the stratification level was at the right

level. These calculations rely on a knowledge of opening sizes and their aerodynamic performance. Buoyancy-driven natural ventilation is characterized by small driving pressures which lead to the need for large openings.

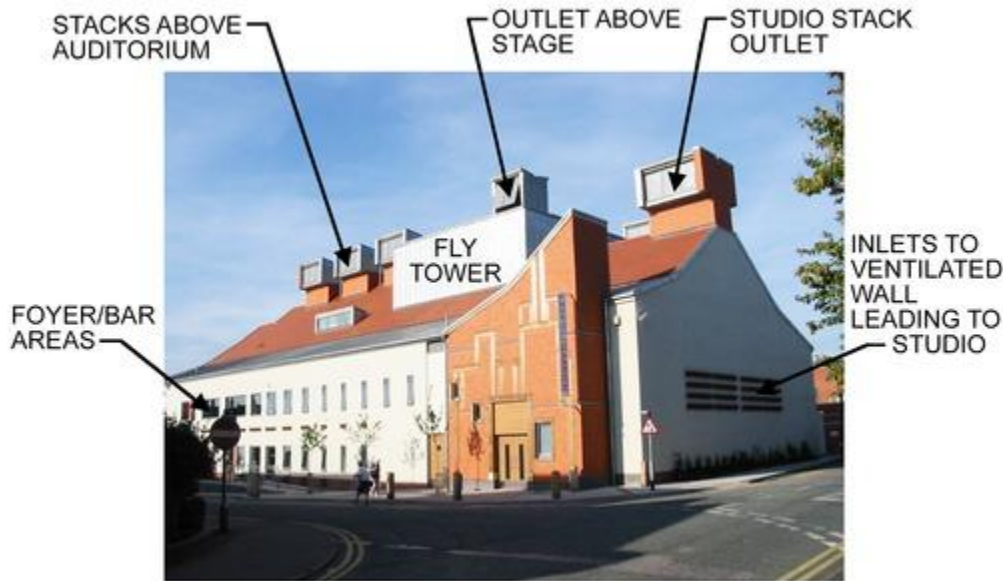


Figure 28. View of Lichfield Garrick from South

The ventilation strategy was designed to passively remove 375,000 Btu/h. This required the provision of a total free area of 388 ft² and was achieved using a plenum below each of the seating rakes, supplied with outdoor air from three sides of the building. A duct leading from above the rear stalls to the ceiling above the balcony seating avoids the build-up of warm, trapped air below the balcony that would diminish the effect of the thermal mass in that area. Outflow paths are provided by eight large stacks, mounted along two ridge lines on the roof ([Figure 28](#)).

Geometry and Mesh Generation

Both the geometry and the mesh were generated using the preprocessing tools available in the software package. When modeling natural ventilation in CFD, it is essential to accurately model the effects of flow through the openings. One approach is to model some proportion of the external space, thus removing the need to specify boundary conditions at the opening boundaries. However, this requires more computation and detailed information about the geometry and components that comprise the inlets and outlets. As an alternative, the boundary here was defined at the point at which air enters and leaves the auditorium, and conditions specified to represent the effects of components such as louvers, dampers, attenuators, and heating elements at openings.

The mesh used in this simulation was a structured Cartesian grid. Such meshes can reduce the computational overhead required by unstructured meshes and avoid some of the numerical instabilities during the iterative solution procedure.

Boundary Conditions and Solver Techniques

Predicted pressure drops across components at inlets and outlets were used in the orifice flow equation (see [Chapter 16 of the 2021 ASHRAE Handbook—Fundamentals](#)) to determine a discharge coefficient C_d to represent resistance to flow at openings. For any openings where pressure loss data were unavailable, a discharge coefficient of 0.6 was used, representing the effect of a sharp-edged orifice. In these cases, it was necessary for the design team to ensure that the combination of free opening area and discharge coefficient in the final design provided at least as much airflow as the combination used in the CFD simulations.

Heat gains are generated by occupants (205,000 Btu/h) and lighting (136,000 Btu/h). These were modeled as convective gains into the domain. However, to account for the convective/radiative split, 50% and 10% of the occupant and lighting gains (respectively) were assumed to be radiated to the surrounding surfaces from where they were convected into the domain. Buoyancy was modeled using the Boussinesq approximation (Gray and Giorgini 1976), which assumes density to be constant everywhere except in the source term of the momentum equation.

Turbulence is modeled using the k - ϵ model with constants derived from renormalisation group theory (ASHRAE *Standard* 55). This model was used, because it was found to more accurately predict entrainment into the buoyant plumes, which are known to determine the key characteristics of these flows (e.g., interface height, temperature of stratified layer) (Cook and Lomas 1998). Validation of the CFD techniques described here was conducted using analytical and experimental models as described in Cook and Lomas (1998).

Convergence Criteria

Convergence was deemed to have been achieved when the residual in the enthalpy equation, in watts, was less than 1% of the total heat convected into the domain at the heat sources, and when the absolute values of variables at the user-defined monitoring point did not change by more than about 0.1% over approximately 20 iterations. The monitoring point used in this case was located just below the roof outlets in the auditorium. Convergence was successfully achieved according to these criteria, using under-relaxation in the form of false time steps. This type of convergence control uses the local cell size and a characteristic time scale for the flow evolution to define under-relaxation factors, which vary throughout the domain. False time step values of 0.1s were used for each of the three momentum equations.

Results

The simulation predicted a stable stratification in which the occupied zone is bathed in the air at, or just above, the ambient temperature (see [Figure 29](#)). This illustrates one of the key advantages of buoyancy-driven displacement ventilation, whereby the height of the stratified layer is determined by the ventilation opening sizes, not by the amount of heat gain in the space. The system can be thought of as self regulating because any increase in heat gain increases the temperature of air in the stratified layer, which increases the driving force, and hence the flow rate through the building, as required. In this case, the layer of stratified air drives a flow of 8.3 ach through the main auditorium, equivalent to about 45 cfm per person. This is typical for naturally ventilated buildings of this type and is necessary to provide thermal comfort, as well as an adequate supply of fresh air.

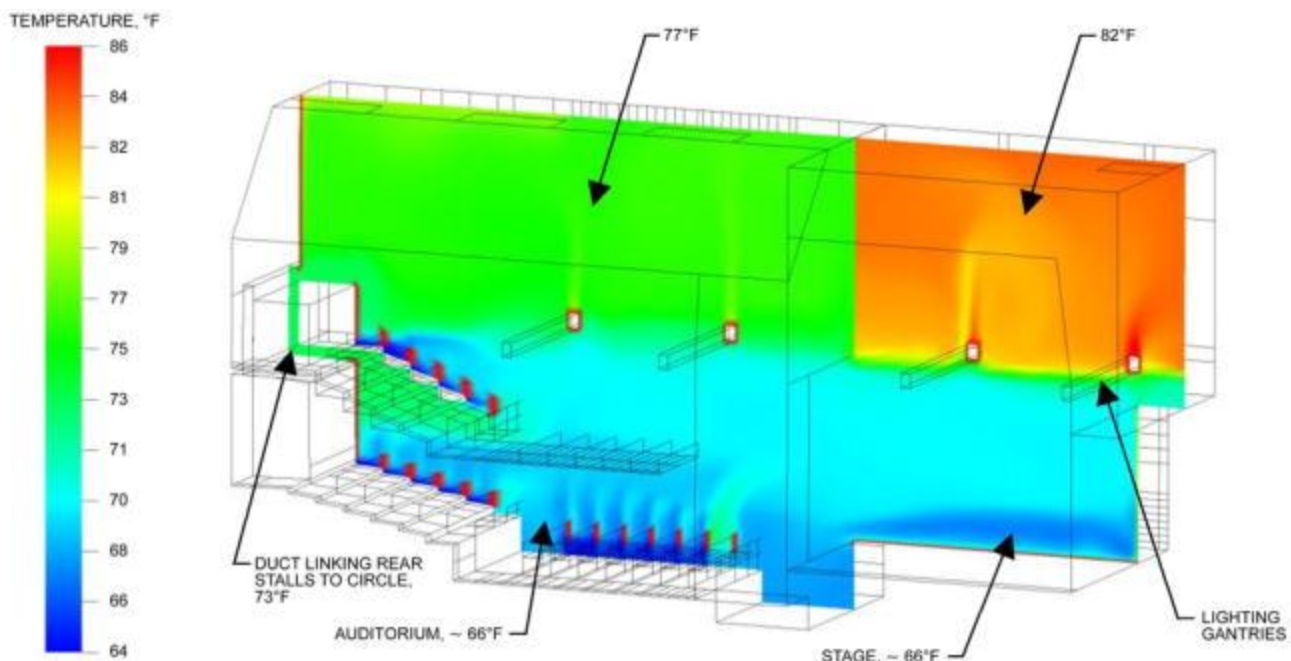


Figure 29. Temperature Prediction over Vertical Plane in Auditorium

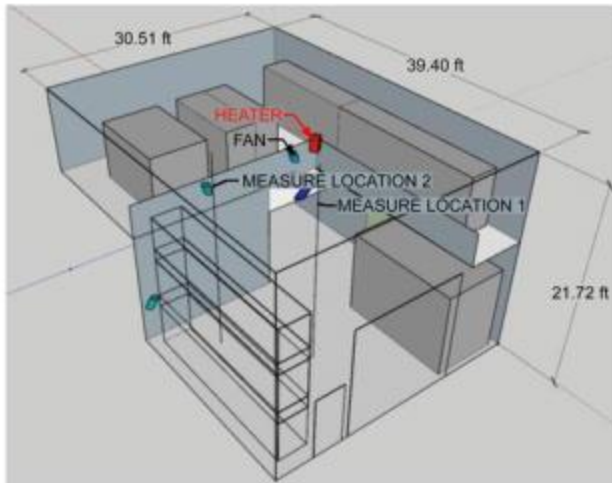
3.7 INDUSTRIAL WAREHOUSE

In large industrial warehouses, thermal stratification can be significant, resulting in buoyancy-dominant indoor airflows. A typical vertical temperature gradient was reported to be 10.3°F/ft (Forrest and Owen 2010) to 10.5°F/ft (Aynsley 2007). As a result, the accumulation of hotter air at higher sections elevates heat flux through surrounding walls and roofs, one of the major warehouse energy wastages. Severe thermal stratification is also a concern for temperature-sensitive goods and products (Li 2016). ASHRAE (2008) recommends thermal destratification for climate zones 5 to 8 of North America, using fans, high-velocity vertical-throw duct diffusers, and air-rotating devices. Examples of thermal destratification energy savings include 26.4% reduction in gas usage (Aynsley 2005) and 19.3% reduction of heating energy (Armstrong et al. 2009) in some cases. In recent years, warehouse thermal stratification and destratification have garnered more attention, mostly as a result of the booming e-commerce industries and their integration with conventional retailers, especially in China and other East Asian countries. CFD is an important technique for analysis of thermal stratification and destratification strategies in warehouses. One of the major challenges, however, is choosing the suitable CFD method for modeling air heating and mixing devices (e.g., ceiling rotating fans, wall-mounted bucket-type axial fans and forced air heaters). This example applies CFD to real-world, large industrial spaces, with the focus on heating and mixing devices, acquiring boundary conditions from the field, and analyzing the simulation results for the energy performance evaluations.

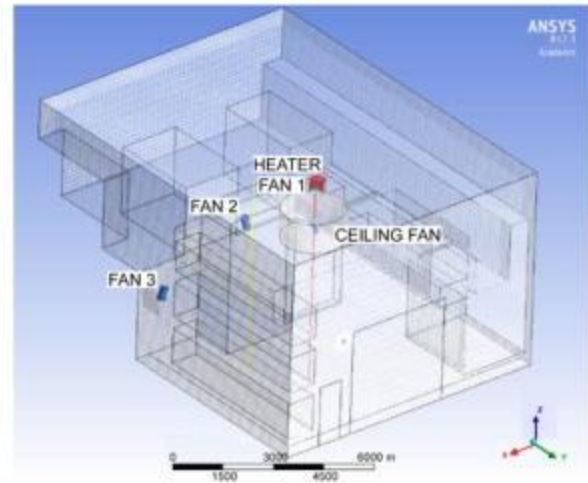
Geometry Generation

This example includes two actual warehouses: the QT and KS buildings. The QT building is a storage warehouse with a size of $39 \times 30.5 \times 22$ ft ($L \times W \times H$), with about half of the space divided horizontally into two sections (an upper section and a ground section) to maximize storage space, as shown in [Figure 30A](#). The existing QT warehouse was equipped with a 51,000 Btu/h electronic forced-air heater beneath the ceiling, and a 670 cfm ceiling bucket fan. The current analysis added a 160 rpm ceiling rotating mixing fan for the evaluation of potential destratification improvement.

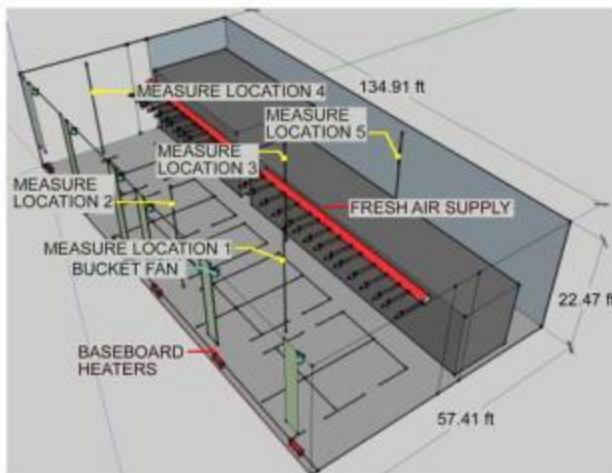
The KS warehouse ([Figure 30C](#)) is a larger building, $135 \times 57 \times 23$ ft, heated by a mechanical duct diffuser system and six 3400 Btu/h baseboard heaters at the ground level under the windows. The conditioned air from every duct diffuser is projected horizontally into the space at 100 cfm per outlet, at a constant 104°F. Six 670 cfm bucket fans were installed above the baseboard heaters for destratification.



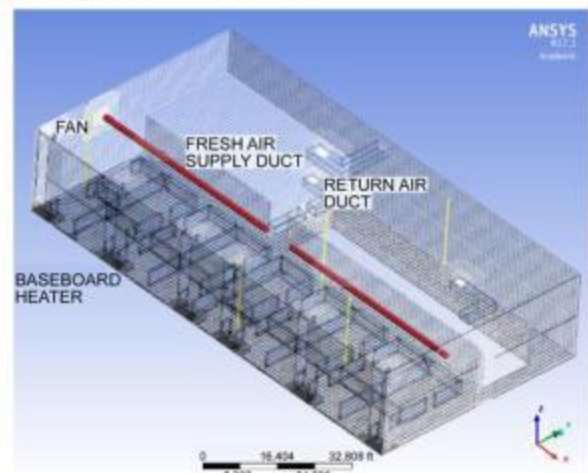
(A) 3-D VIEW OF QT WAREHOUSE.



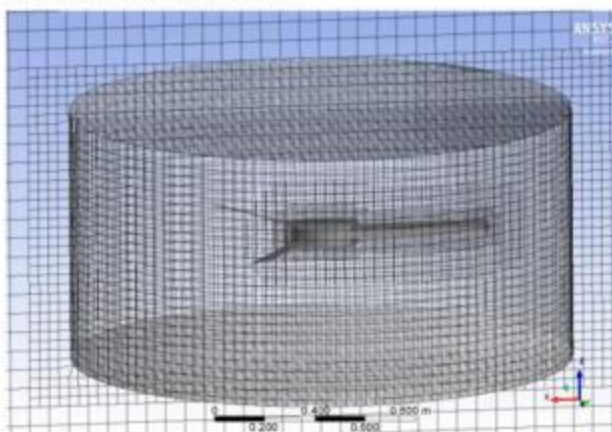
(B) CFD MODEL OF QT WAREHOUSE.



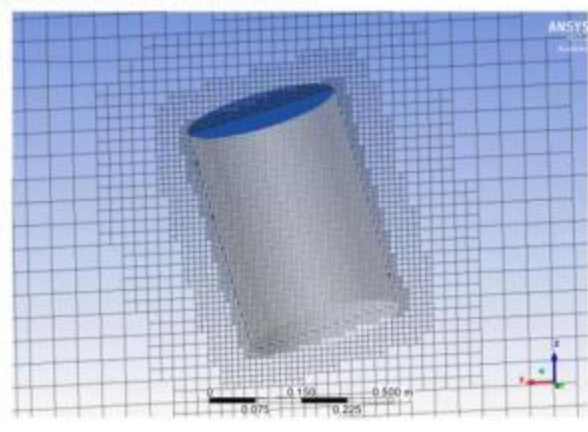
(C) 3-D VIEW OF KS WAREHOUSE.



(D) CFD MODEL OF KS WAREHOUSE.



(E) MESH OF CEILING ROTATING FAN.



(F) MESH OF BUCKET WALL.

Figure 30. View Models and CFD Models of Warehouses

General geometrical information was collected, including the dimensions of the warehouses, the size of the doors and windows, connections to neighboring rooms or buildings, and storage rack layouts and dimensions. Here, a commercial CFD software package was used. Most of the storage racks and shelves were modeled by solid blockages, but the mixing devices and HVAC ducts were modeled as their original cylinder shapes. Internal partitions were modeled as zero-thickness blockages because no heat transfer calculation was needed for internal structures. The ceiling rotating fan was modeled in detail to reflect the real-world unit, considering the fan blade diameter of 4.3 ft and a curve surface with a 1.15 ft radius arc; the chord of each blade has a 15° angle with the horizontal plane (Momoi et al. 2004). [Figure 30E](#) shows the CFD model of the ceiling rotating fan, and [Figure 30F](#), the bucket fan.

Mesh Generation

Both warehouse models are meshed mostly by Cartesian cut-cell grids first in the software. For regions with heaters and fans, more detailed localized meshes were created to provide enough resolutions considering the existences of strong gradients. [Figures 30E](#) and [30F](#) show the local mesh examples for the ceiling rotating fan and the bucket fan models. To model the rotating fan, the whole model was divided into two parts: the cylindrical section encompassing the fan and rotating at a speed of 160 rpm, and a stationary section, as shown in part E of the figure. The bucket axial mixing fan was modeled by a constant-pressure jump fan model at a set volumetric flow rate ([Figure 30F](#)). The forced air heater (not shown) was also modeled by the pressure jump fan model with a constant heat source, following the method proposed by Forrest and Owen (2010). For more detailed CFD setups, see Wang and Li (2017). For the KS building, similar mesh refinement treatments were applied to the baseboard heaters and near the HVAC duct supplies, as shown in [Figure 30D](#). As a result, a total mesh of 7.5 ft was created for the QT and KS buildings.

Solvers and Models

To model buoyancy-driven flows in such large spaces, a real gas model with temperature varying density was used. For the turbulence effects, the standard k - ϵ two-equation turbulence model has been found effective by previous studies (Li et al. 2009). Momoi et al. (2004) also found the standard k - ϵ model adequate for modeling ceiling rotating fans.

Boundary Conditions

The thermal resistance properties of building envelopes were collected from the owners or engineers. For CFD simulations of large spaces, various thermal boundary conditions are available for modeling solid surfaces: constant temperatures, heat transfer coefficients, and heat fluxes. For modeling actual warehouse envelopes, the constant heat transfer coefficient boundary conditions were more reasonable for modeling both interior and exterior surfaces. The estimation of the convective heat transfer coefficients h_c was based on the models suggested by Qi et al. (2013) as a function of temperature differences, surface orientations, and Reynolds and Prandtl numbers. For other surfaces (e.g., the ground), constant temperatures were applied. For the duct diffusers, constant velocity and temperature were modeled using the data available from the on-site HVAC monitoring systems. [Table 4](#) provides the key boundary condition settings.

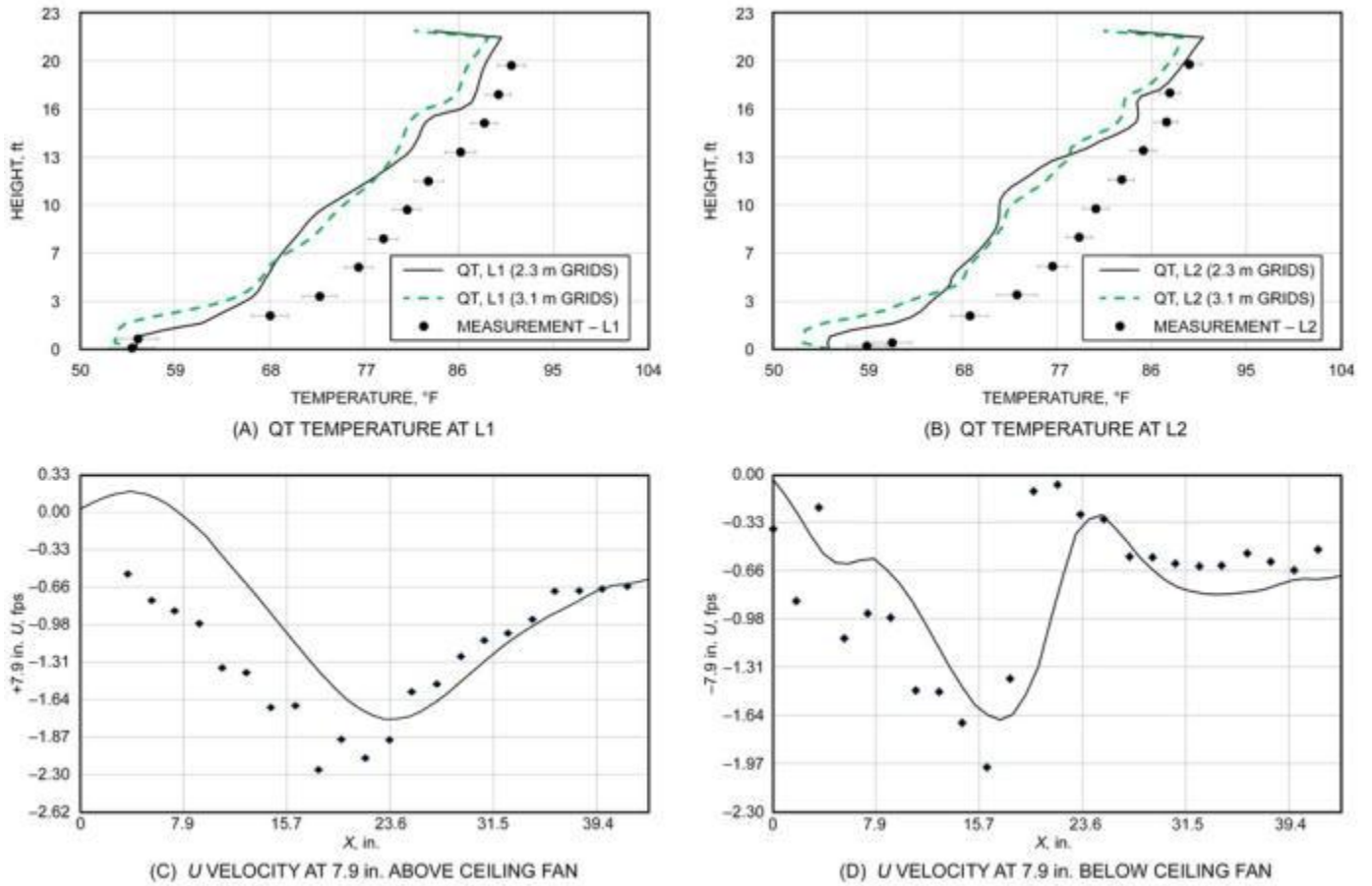


Figure 31. Temperature Validation for Two Locations in QT, and Velocity Validation for Modeled Ceiling Rotating Fan Using Literature Data (Momoi et al. 2004)

Convergence/Grid Independence

A grid sensitivity study was conducted for the QT warehouse using 7.5 ft cells and 10.1 ft cells. For the KS warehouse, the total grid number was also chosen to be 2.3 million.

Results

Different thermal destratification strategies were simulated, as shown in [Table 5](#). For the QT warehouse, two more bucket fans were added: a second fan, to the left of the existing, first fan, and a third fan, close to the wall, with the supply air pointing upwards towards the ceiling. A ceiling rotating fan was also added, as shown in [Figure 30B](#). Validation results of temperature and velocity profiles are shown in [Figure 31](#). Including the existing system q_1 , a total of six different combinations of fan operating strategies were simulated from q_1 to q_6 . For the KS warehouse, different bucket fan operating speeds (all off, 30%, and 100%) and air supply directions from the duct diffusers (horizontal throw, vertically downward supply, and 45° downward supply) were simulated by a total of five cases from k_1 to k_5 ([Table 5](#)).

To quantify the level of thermal stratification, the nonuniformity coefficient θ is defined with [Equation \(2\)](#): a greater value of θ indicates a stronger stratification.

$$\theta = \frac{\sqrt{\sum_{i=1}^n (T_i - T)^2 / (n - 1)}}{T} \quad (2)$$

where

n = total number of temperature data measured vertically at specific location in space

T_i = temperature at location i

T = average temperature

[Figure 32A](#) compares the nonuniformity coefficients for all six cases of the QT warehouse. Comparing the cases with bucket fans running (q_1 , q_4 , q_5 , and q_6) and off (q_2) demonstrated a clear improvement in mixing when the fan was running. For the bucket fan flow direction, pushing air downwards (q_1) was better than sending air upward through the bucket fan (q_4): $\theta \approx 0.23$ in q_1 , and $\theta = 0.38$ in q_4 . Therefore, it is more beneficial to use a bucket fan close to the

roof heating source with downward air than a wall-mounted bucket fan blowing air upwards, which also causes a potential increase of ceiling heat transfer. The q_1 case was the worst thermal stratification case: the resultant roof heat loss was found to be about 9900 Btu/h, as shown in Figure 32B. Applying a destratification strategy (e.g., the best case of q_3), the energy saving can be 3800 Btu/h in q_3 , a reduction of around 40% compared to q_1 . Energy savings from other strategies also found that a lower θ result in a less heat loss through the roof.

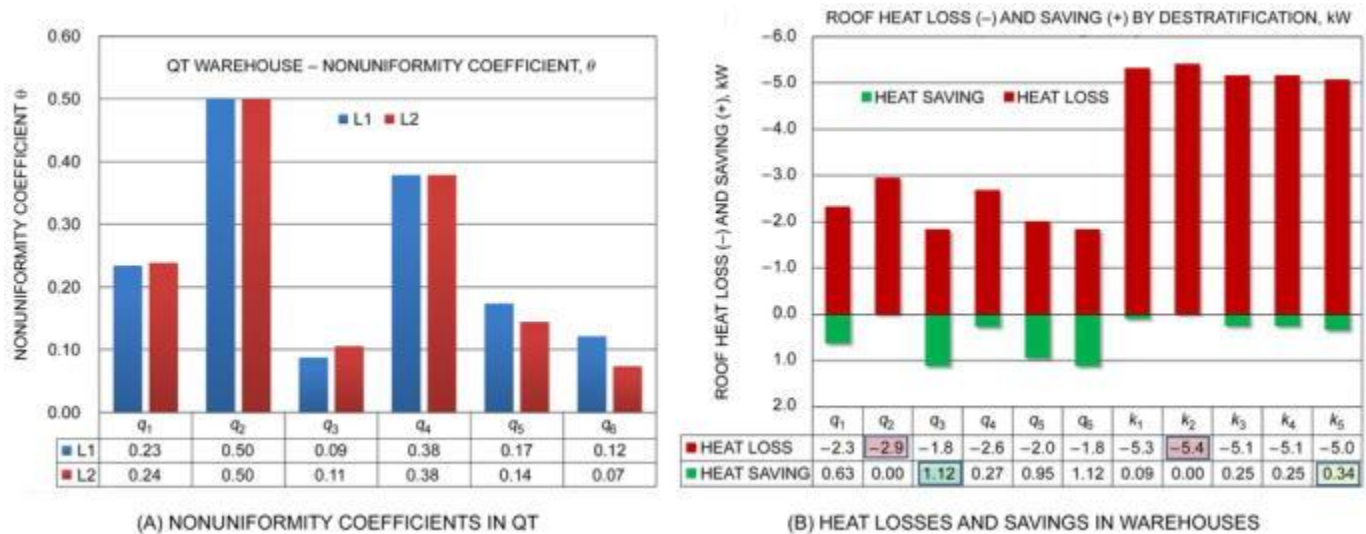


Figure 32. Comparison of Nonuniformity Coefficients, Heat Losses, and Savings in Warehouses

Table 4 CFD Simulation Thermal Properties and Boundary Conditions

CFD Settings	QT Warehouse	KS Warehouse
Ambient temperature, °F	-6.7	19.9
Ground	Constant temperature 55°F	Constant temperature 70°F
Interior wall	R5	Constant temperature 75.2°F
Convective heat transfer h_c	Roof: 2.75 Btu/h · ft ² · °F Wall: 3.65 Btu/h · ft ² · °F	Roof: 0.60 Btu/h · ft ² · °F Wall: 1.69 Btu/h · ft ² · °F
Other surfaces	Constant temperature 68°F	Constant temperature 76.6°F
Air heater	Ceiling air heater: 51,177 Btu/h	6 baseboard heaters: 3,412 Btu/h/each
Ceiling rotating fan	Diameter: 4.3 ft; 160 rpm	N/A
Bucket fan	Diameter: 1.152 ft; Height: 1.240 ft; 670 cfm	
Diffuser	N/A	33.96 fps of 74°F air

The calculated nonuniformity coefficients of the KS warehouse are all less than 0.1, ranging from 0.006 to 0.096 (not shown here). This shows that, although the KS warehouse is about seven times larger than the QT, using ceiling duct diffusers and many wall-mounted bucket fans significantly overcomes the thermal stratification. The corresponding energy saving from ramping up fan speed is only 2% for k_1 and 5% for k_3 when using k_2 as the baseline, as shown in Figure 32B. Therefore, using duct diffusers already ensures a good mixing, and increasing mixing fan speed is unnecessary in this case. A more effective way to further reduce thermal destratification is to change the diffuser air supply angles (at zero extra energy costs). When the diffuser supply air is changed from horizontal throw in k_1 (the existing system) to 45° downwards in k_4 and, further, to vertically downward (90°), the corresponding energy saving is 5% in k_4 and over 6% in k_5 (a similar scale as, or slightly better than, adjusting bucket fan speed). Therefore, for both warehouses, a preferred thermal destratification strategy is always to actively deliver warm conditioned air effectively to the lower portion of the building, rather than passively relying on local mixing devices (e.g., wall mounted bucket fans), which are often complicated by issues of location and number of units used. An exception is the ceiling-mounted rotating fan in the QT warehouse, which was found to be a superior destratification method. This example demonstrated that using CFD techniques can effectively aid the design and analysis of thermal stratification and destratification in warehouses.

Table 5 Destratification Strategies in Warehouses

Warehouse	Case	Destratification Strategy
QT	q_1 (existing system)	Bucket fan #1 on with air blowing downwards

	q_2	All fans off
	q_3	Only ceiling fan on, bucket fans off
	q_4	Bucket fan #3 on with air blowing towards roof
	q_5	Bucket fan #1 and #2 on
	q_6	Bucket fan #1, #2, and #3 on
KS	k_1 (existing system)	All bucket fans at 30% speed, horizontal diffuser air
	k_2	All fans off, horizontal diffuser air
	k_3	All fans at 100% speed, horizontal diffuser air
	k_4	All fans at 30% speed, 45° downward diffuser air
	k_5	All fans at 30% speed, vertical downward diffuser air

4. MULTIZONE SIMULATION METHOD

Multizone modeling differs from CFD in that it considers a macro view of a building, as opposed to a micro view. CFD provides detailed transport characteristics in a given building volume, but multizone modeling provides building-wide characteristics of an entire building volume. Multizone airflow and contaminant transport models treat a building as (1) a system of interdependent nodes (or zones) that store air and (2) contaminant mass and transport elements (or links) that carry mass between the nodes. Zones in a model constitute by individual rooms, plenums, and duct junctions, and examples of links include windows, doors, envelope leaks, and duct segments. Nodes are considered to be well mixed (i.e., characterized by single, representative properties including temperature, pressure, and contaminant concentrations). However, pressure is allowed to vary within each zone hydrostatically.

Interzone and infiltration airflows are determined by calculating the interior zone pressures that satisfy mass balance in each zone, based on driving forces and boundary conditions that include HVAC system airflows, as well as wind and stack pressures exerted on the building envelope. Once the airflows are obtained, contaminant sources and removal mechanisms (e.g., deposition, filters) are accounted for in a contaminant mass balance to determine the time history of contaminant concentration over the simulation period. The fundamentals of multizone simulation are discussed in [Chapter 13 of the 2021 ASHRAE Handbook—Fundamentals](#).

4.1 MULTIZONE SIMULATION OF A TYPICAL OFFICE BUILDING

This example uses multizone modeling to evaluate indoor air quality (IAQ) and ventilation for a medium-sized office building. More specifically, this case demonstrates that multizone modeling can show the effects of building envelope leakage on ventilation system performance and average contaminant levels.

Building Description

The building ([Figure 33](#)) is based on a representation of a U.S. Department of Energy (DOE) Commercial Reference Building model developed by Ng et al. (2012). The building measures 165 by 108 ft. Floor and plenum heights are 9 ft and 4.125 ft, respectively, for a total of 39.37 ft. It consists of three floors, each served by a return air plenum located above the occupied level.

Multizone Representation of Building

The multizone representation of the building is shown in [Figure 33](#). Each floor was subdivided to include five occupied zones: a core zone and four perimeter zones. This zoning strategy reflects that of the original DOE energy model upon which it is based, which treats the perimeter zones separately due to orientation-based solar loads and the core zone having a different energy load from the perimeter zones. This zone topology is also practical for the purposes of this example, because it captures the wind-related effects on the perimeter zones and the core/perimeter ventilation system layout. The core zone was slightly modified from the original model so that each floor includes a stairwell, elevator, and restroom. The stairwell and elevator span the entire height of the building to allow consideration of stack-driven flows through these vertical shafts.

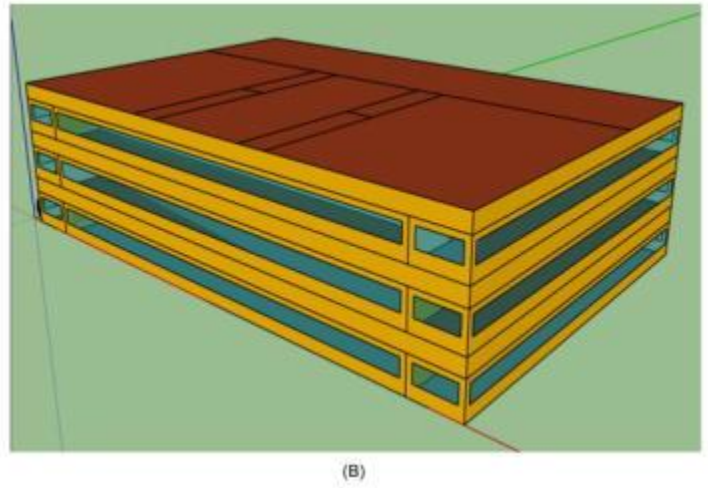
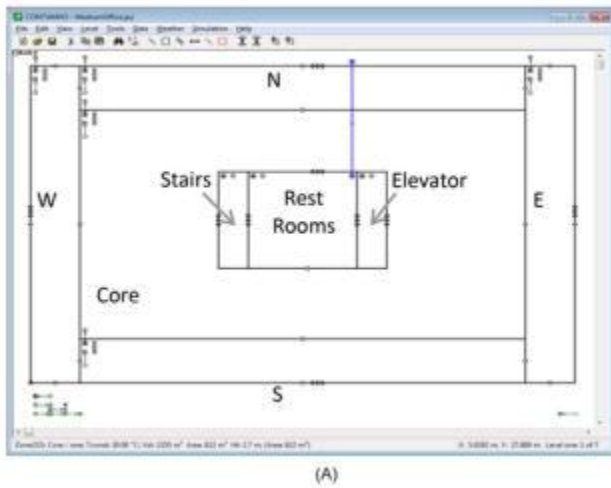


Figure 33. Medium Office Building Model: (A) Schematic Floor Plan and (B) 3D Representation

Airflow characteristics of the building envelope and interior partitions are based on the model described in Ng et al. (2012). Exterior envelope leakage is defined using an effective leakage area of $0.08 \text{ in}^2/\text{ft}^2$ at a reference pressure of $0.08 \text{ lb}/\text{ft}^2$, a discharge coefficient of 1.0, and a pressure exponent of 0.65. The leakage between the perimeter and core zones are defined as open office plans to reduce interzone resistance to airflows, and the ceiling plenum was connected to the occupied zones with orifice areas of 10 ft^2 per 1000 ft^2 of ceiling area. Wind pressure coefficient profiles were specified based on low-rise buildings, as defined by Swami and Chandra (1988), and the building was situated in a suburban location to yield a surface-averaged wind speed modifier of 0.36 (Walton and Dols 2006). Simulations were run using a TMY3 weather file for Baltimore, MD.

Each floor of the building is served by a single air handler, and each restroom is served by a dedicated exhaust system. Two ventilation systems were modeled in this example: a constant-air-volume (CAV) mechanical ventilation system and a CAV system that also incorporates CO_2 -based demand-controlled ventilation (DCV). The restrooms were exhausted at a constant rate of 212 cfm in both systems.

Source for Contaminant Model

Contaminants were simulated to represent both indoor and outdoor sources. The selected contaminants enable the investigation of the effects that various ventilation system and building leakage characteristics have on different types of sources. Occupant-generated carbon dioxide (CO_2) was included to model demand-controlled ventilation, because it can be used as an indicator of people being present in the building and thus as a controlled variable for establishing ventilation airflow rates. Volatile organic compounds (VOCs) were simulated to represent a generic indoor source associated with building materials and occupant activities. Particulates less than $2.5 \mu\text{m}$ in diameter ($\text{PM}_{2.5}$) were simulated to represent an outdoor source. The properties of these contaminants, sources, and sinks are based on those provided in Ng et al. (2012).

- CO_2
 - Outdoor concentration: 354 ppmv
 - Indoor generation rate: 0.01 cfm per person
- VOC
 - Outdoor concentration: $0.0 \mu\text{g}/\text{ft}^3$
 - Indoor generation rate: 0.5 mg/h
- $\text{PM}_{2.5}$
 - Outdoor concentration: $0.5 \mu\text{g}/\text{ft}^3$
 - Indoor generation rate: N/A
 - Deposition rate: 0.5 h^{-1}

Simulation Results

Multizone modeling provides the ability to evaluate ventilation system designs with respect to building envelope tightness using pressure-based airflow network calculations as opposed to assumed and empirically determined air change rates (Ng et al. 2014). [Figure 34](#) provides plots of the CO₂ concentration in the three return plenums. The plot on the left is for the base configuration with a building leakage rate of 0.08 in²/ft², and that on the right is ten times tighter. As shown in [Figure 34](#), there is less variation in the CO₂ concentrations among the three zones in the tighter building, enabling better control of the DCV system.

Calculating airflow and contaminants together allows comparisons between various ventilation systems that use contaminant-based control strategies, evaluating the controlled contaminant (here, CO₂) and the effect of different control schemes on uncontrolled contaminants (here, VOCs and PM_{2.5}). [Figure 35](#) shows the building average VOC concentration for four different combinations of building envelope leakage and ventilation system type: leaky envelope with CAV system, tight envelope with CAV system, leaky envelope with CAV/DCV system, and tight envelope with CAV/DCV system. This plot reveals that the internal concentration is elevated by the lower outdoor air intake rates attributed to the DCV control system for both the leaky and tight envelopes. Thus, even though DCV and tighter building envelope may lead to energy savings by reducing outdoor air intake, this approach could lead to increased occupant exposure of internally generated, uncontrolled contaminants.

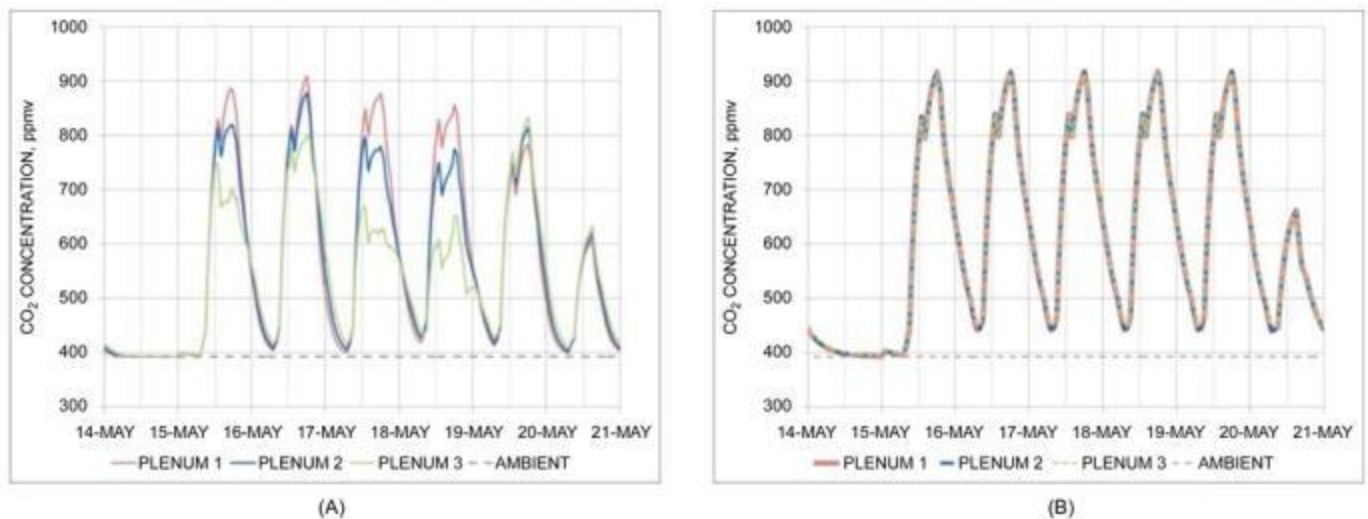


Figure 34. CO₂ Concentration for DCV System in (A) Leaky and (B) Tight Buildings

Further, as mentioned above, building energy measures such as ventilation strategies and envelope leakage rates can affect building energy usage. Multizone energy simulation tools could be used to evaluate the trade-offs between energy conservation strategies and IAQ. Multizone, whole-building energy analysis software can provide a wide range of building energy usage characteristics and has been coupled with various means, including cosimulation, to allow these analyses to be carried out in an integrated manner (Dols et al. 2016; Ng et al. 2018).

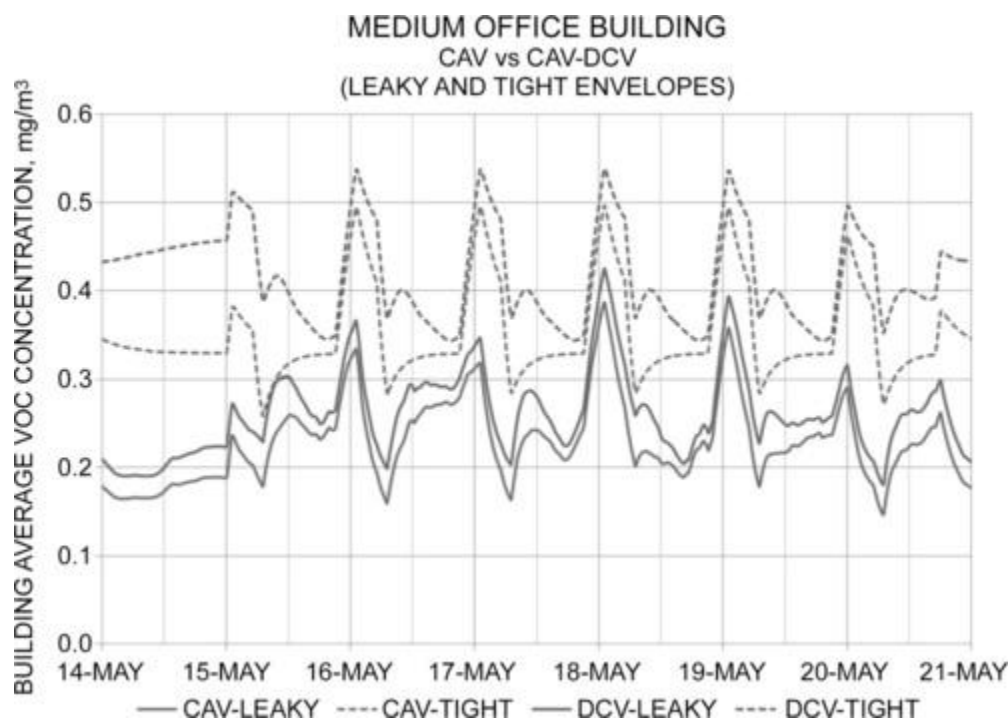


Figure 35. Comparison of VOC Concentrations with Respect to Envelope Leakage and Ventilation System

4.2 MULTIZONE SIMULATION OF AIRBORNE TRANSMISSION RISKS IN A LARGE OFFICE BUILDING

This example shows a multizone modeling approach to evaluate the airborne quanta transmission for the U.S. DOE Commercial Reference Building model developed by Ng et al. (2012) (the large office building). The classic Wells-Riley model was applied to the multizone building and simulated exposure to infectious doses in terms of *quanta* (Yan et al. 2022). A **quantum** was defined as the inhaled dose needed to infect a person. The number of infected occupants bears a Poisson relation to the number of quanta they breathe, which means 63% of occupants will be infected when each occupant breathes one quantum on average. This modeling approach could help quantify the relative benefits of different risk mitigation strategies and compare their effectiveness. The final simulation input project and output files of the US DOE prototype buildings are also shared to apply the same approach to other building types. The files can be downloaded from github.com/CUBEL_eonwang/CONTAM-Multizone-DOE.

Building Description

The building has 12 floors with a footprint of 38,351.8 ft², one basement, and a flat roof. Except for the basement, each floor has a central core zone (25,015 ft² with one staircase, elevator, and restroom located in the middle of the zone, a data center, and the perimeter zones in four directions (Figures 36 and 37). The height from floor to ceiling is 9.0 ft, and the floor-to-floor height is 13.1 ft because of the additional height of the plenum on each floor. Each floor is connected to the top and bottom floors with the staircases, elevator shafts, floor/ceiling leakages, and to the ceiling plenum through one return grill of each zone. Internal wall leakages between every two zones are defined as the three leakage paths at the top, middle, and bottom locations.

Input Parameter Settings

The simulations were conducted for one weekday, December 21, in Chicago. The CONTAM-*quanta* approach was used for evaluating occupants' exposure risks. For a detailed introduction of the method, see Yan et al. (2022). One infected person was assumed to be located in the first-floor core zone during working hours (8:00 – 17:00) without leaving the space. This was one of the worst scenarios with the highest exposure risks. The VAV system started at 6:00 and turned off at 22:00. The CONTAM model was created to match the operation and occupancy schedules of the EnergyPlus model. The detailed input setting is shown in Table 6.

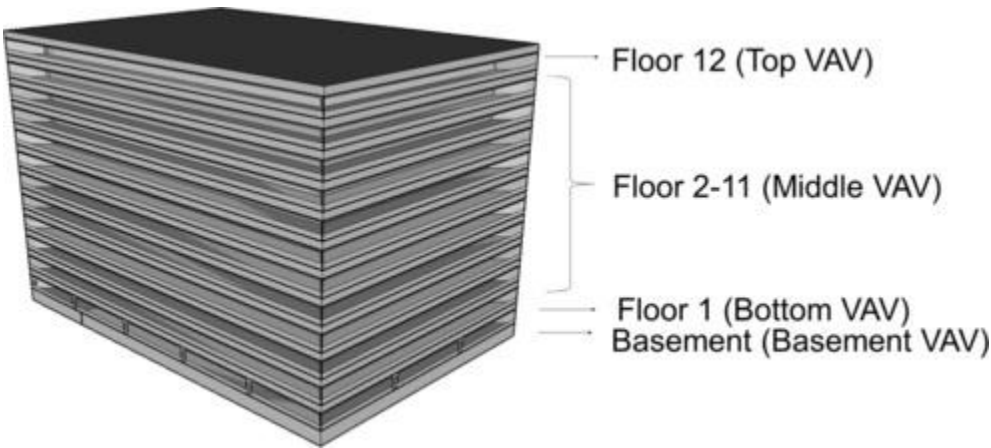


Figure 36. DOE Large Office Prototype Building Model with VAV System Details Shown in Table 7

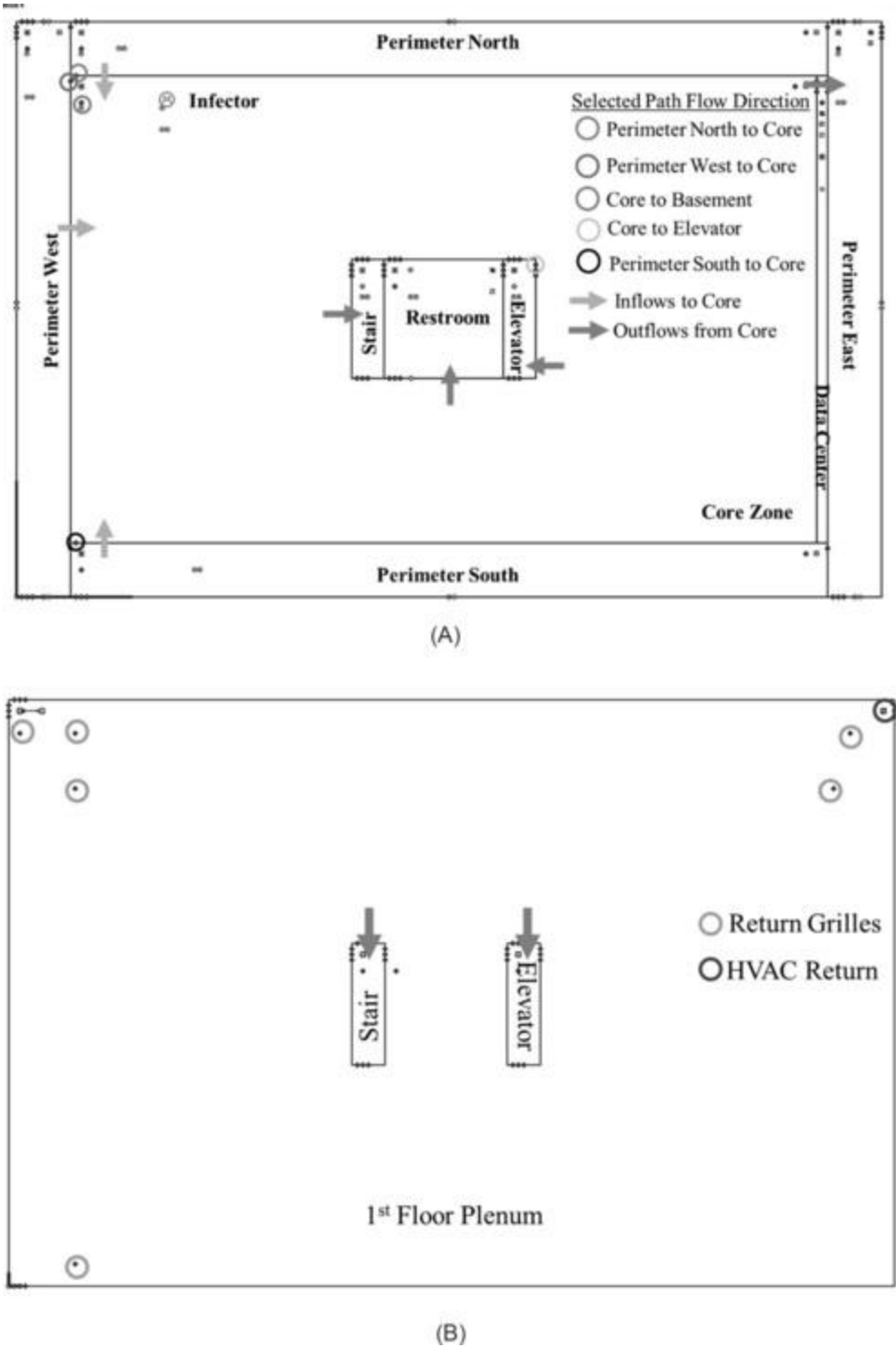


Figure 37. (A) Floor Plan of First Floor of DOE Large Office Prototype Building, and (B) Floor Plan of First-Floor Plenum with Return Grilles and HVAC Return

Table 6 Input Parameters for CONTAM-*quanta* Simulation of DOE Large Office Prototype Building, First Floor Core Zone

Inputs		Parameters		References
Zone geometry	Volume, ft ³ /Area, ft ²	Core	225,166/25,015	Ng et al. (2012)
		Perimeter West (Perimeter East)	21,471/2422	
		Perimeter North (Perimeter South)	28,358/3154	
		Restroom	9782/1087	
		Stairs (Elevator)	2673/297	
		Data Center	3482/388	
Zone occupancy	Infector	1	—	
	Susceptible	133	Ng et al. (2012)	

Initial quanta concentration	Concentration, quanta/m ³	0	—
Quanta generation	Quanta generation rate, quanta/h	65	Buonanno, Stabile and Morawska (2020)
	Breathing rate, m ³ /h	0.72	U.S.EPA (2011)
	Generation duration	8:00 to 17:00 (9 h)	—
Deposition and deactivation	Surface deposition rate	0.3 h ⁻¹	Diapouli, Chaloulakou and Koutrakis (2013); Thatcher et al. (2002);
	Particle deactivation rate	0.63 h ⁻¹	Van Doremalen et al. (2020)
Germicidal ultraviolet light	in-room GUV removal rate	4 h ⁻¹	Miller and MacHer (2000)
	in-duct GUV removal efficiency	87%	Kujundzic, Hernandez and Miller (2007)
	MERV8 removal efficiency (baseline – BL)	20%	NAFA Technical Committee (2018)
MERV removal	MERV11 removal efficiency	65%	
	MERV13 removal efficiency	85%	
AC airflow rates	PAC1	975 cfm	From manufacturer
	PAC2	2140 cfm	
	PAC3	3075 cfm	
	PAC4	36,000 cfm	
	HEPA removal efficiency	99%	Miller-Leiden et al. (1996)
Mask	Mask wearing percentage	0 or 100%	—
	Exhale removal efficiency	50%	Pan et al. (2021)
	Inhale removal efficiency	30%	

Simulation Results

[Figure 38A](#) reports the simulated transient quanta concentrations in all zones of the first floor when the infector was located in the first-floor core zone ([Figure 37A](#)). For the baseline (BL) case (MERV8+BL OA), during the initial two hours (8:00 – 10:00 am), the quanta concentration accumulated in the zones rapidly; it reached steady state after 10:00. [Figure 38B](#) shows the accumulated individual exposure risk for an occupant in different zones on the first floor over the working hours. At the end of the nine working hours, the infection risk is less than 2% in the core zone (source zone), 1.6% in the restroom, about 1% in the elevator shaft, stair and datacenter, and less than 0.7% in all other ones of the first floor.

Table 7 VAV Information

VAV System	Basement	Floor 1	Floor 2-11	Floor 12
Supply/return, cfm	9810/8836	24,685/22,227	20,002/17,989	21,888/19,706
Baseline OA, %	26	14	17	16

The results of predicted exposure risks for the occupants' nine-hour exposures in the first-floor core zone are demonstrated in [Figure 38C](#). The acceptable risk level ($R_0 = 1$) was calculated to be 0.75% for this zone. For the baseline case, the exposure risk was estimated to be 1.83% without mask wearing. By increasing the OA rate to 1.3BL, 2BL, or 100% fresh air, the exposure risk would drop to 1.79%, 1.66%, and 1.12%, respectively. The upgrade of the MERV8 filter in the baseline case to a MERV11 or MERV13 reduces the risk to 1.30% and 1.22%. Adding germicidal ultraviolet (GUV), in-duct GUV (UV-duct) would decrease the baseline exposure risk to 1.19%, while room GUV (room-UV) could lower the risk to 0.89%. For each of the mitigation strategies, the relative risk reduction compared to the baseline is shown in [Figure 38D](#). Upgrading the MERV filters from MERV8 to MERV11 and MERV13 tend to be more effective than adding portable air cleaners (PACs) (PAC1 to PAC3, from 975 cfm to 3072 cfm). The use of MERV13 and in-duct GUV with the Baseline OA provides similar performance to that of 100% OA. When the 100% OA strategy is adopted, the most relative reduction compared to baseline that can be achieved is 40%; to reduce the risk even further, in-zone strategies need to be adopted also such as operating PACs or in-room GUV light.

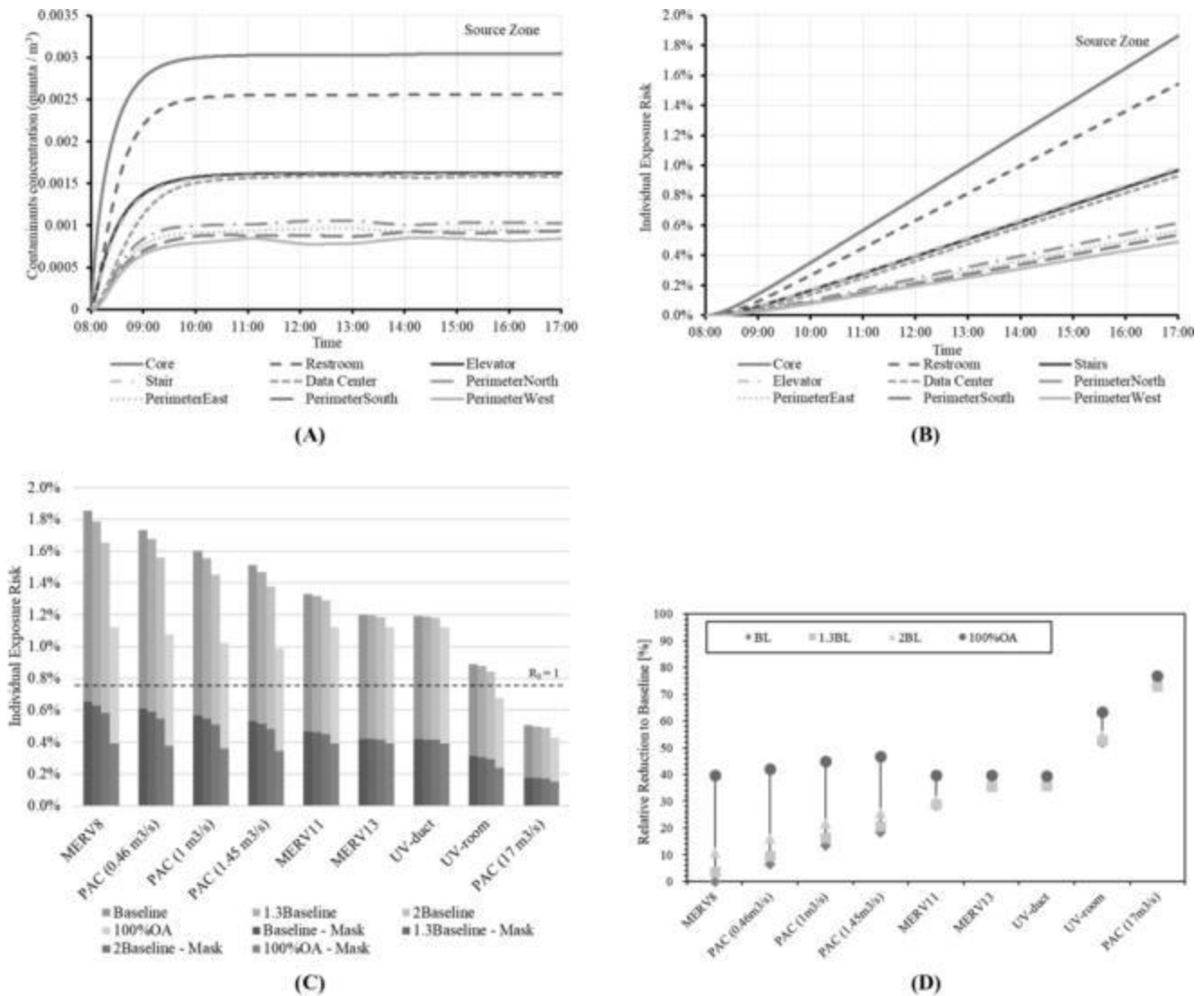


Figure 38. (A) Transient Airborne Quanta Concentrations during Working Hours; (B) Transient Exposure Risks for Occupant in Zones of First Floor; (C) Individual Exposure Risks under Different Combined Mitigation Strategies; (D) Relative Risk Reduction Compared to Baseline Case

REFERENCES

- ASHRAE members can access *ASHRAE Journal* articles and ASHRAE research project final reports at technologyportal.ashrae.org. Articles and reports are also available for purchase by nonmembers in the online ASHRAE Bookstore at www.ashrae.org/bookstore.
- Abdelmaksoud, W.A., H.E. Khalifa, T.Q. Dang, R.R. Schmidt, and M. Iyengar. 2010. Improved CFD modeling of a small data center test cell. Published in *2010 12th IEEE Intersociety Conference on Thermal and Thermomechanical Phenomena in Electronic Systems*, pp. 1-9. [dx.doi.org/10.1109/ITHERM.2010.5501425](https://doi.org/10.1109/ITHERM.2010.5501425).
- Armstrong, M., B. Chihata, and R. MacDonald. 2009. Cold weather destratification energy savings of a warehousing facility. *ASHRAE Transactions* 115(2).
- ASHRAE. 2017. Thermal environmental conditions for human occupancy. *ANSI/ASHRAE Standard 55-2017*.
- ASHRAE. 2016. Energy standard for data centers. *ANSI/ASHRAE Standard 90.4-2016*.
- ASHRAE. 2008. *Advanced energy design guide for small warehouses and self-storage buildings: 30% energy savings*.
- Aynsley, R. 2005. Saving heating costs in warehouses. *ASHRAE Journal* 47(12):46-50.
- Aynsley, R. 2007. Circulating fans for summer and winter comfort and indoor energy efficiency. *Environment Design Guide* TEC 25. Australian Institute of Architects.
- Buonanno, G., L. Stabile, and L. Morawska. 2020. Estimation of airborne viral emission: Quanta emission rate of SARS-CoV-2 for infection risk assessment. *Environment International* 141. doi.org/10.1016/j.envint.2020.105794
- Chen, Q., and J. Srebric. 2002. A procedure for verification, validation, and reporting of indoor environment CFD analyses. *HVAC&R Research (now Science and Technology for the Built Environment)* 11(2):201-216. [dx.doi.org/10.1080/10789669.2002.10391437](https://doi.org/10.1080/10789669.2002.10391437).
- Chen, Q., L. Glicksman, X. Yuan, S. Hu, and X. Yang. 1999. Performance evaluation and development of design guidelines for displacement ventilation (RP-949). ASHRAE Research Project RP-949, *Final Report*.

- Chen, Q., K. Lee, S. Mazumdar, S. Poussou, L. Wang, M. Wang, and Z. Zhang. 2010. Ventilation performance prediction for buildings: Model assessment. *Building and Environment* 45(2):295-303. [dx.doi.org/10.1016/j.buildenv.2009.06.008](https://doi.org/10.1016/j.buildenv.2009.06.008).
- Cook, M., and K.J. Lomas. 1998. Buoyancy-driven displacement ventilation flows: Evaluation of two eddy viscosity turbulence models for prediction. *Building Services Engineering Research and Technology* 19(1): 15-21.
- Cook, M., and A. Short. 2005. Natural ventilation and low energy cooling of large, non-domestic buildings—Four case studies. *International Journal of Ventilation* 3(4):283-294.
- Diapouli, E., A. Chaloulakou, and P. Koutrakis. 2013. Estimating the concentration of indoor particles of outdoor origin: A review. *Journal of the Air & Waste Management Association* 63(10):1113-1129. doi.org/10.1080/10962247.2013.791649.
- Dols, W.S., S.J. Emmerich, and B.J. Polidoro. 2016. Using coupled energy, airflow and IAQ software (TRNSYS/CONTAM) to evaluate building ventilation strategies. *Building Services Engineering Research and Technology* 37(2):163-175.
- Etheridge, D.W., and M. Sandberg. 1996. *Building ventilation: Theory and measurement*. John Wiley & Sons, Hoboken, NJ.
- Forrest, J., and I. Owen. 2010. *MegaFan warehouse case study: Final report*. University of Liverpool.
- Gorst, T. 2003. Civil lifecycles. Short and associates in lichfield. *Architecture Today* 143(2013):34-46.
- Gray, D.D., and A. Giorgini. 1976. The validity of the Boussinesq approximation for liquids and gases. *International Journal of Heat and Mass Transfer* 19(5):545-551. [dx.doi.org/10.1016/0017-9310\(76\)90168-X](https://doi.org/10.1016/0017-9310(76)90168-X).
- Healey, C., X. Zhang, and J.W. VanGilder. 2014. System and method for measurement aided prediction of temperature and airflow values in a data center. U.S. Patent 8,725,307.
- Kujundzic, E., M. Hernandez, and S.L. Miller. 2007. Ultraviolet germicidal irradiation inactivation of airborne fungal spores and bacteria in upper-room air and HVAC in-duct configurations. *Journal of Environmental Engineering Science* 6:1-9. doi.org/10.1139/s06-039.
- Li, Q., A. Mochida, B. Lei, Q. Meng, L. Zhao, and Y. Lun. 2009. CFD study of the thermal environment in an air-conditioned train station building. *Building and Environment* 44(7):1452-1465. [dx.doi.org/10.1016/j.buildenv.2008.08.010](https://doi.org/10.1016/j.buildenv.2008.08.010).
- Li, W. 2016. *Numerical and experimental study of thermal stratification in large warehouses*. M.A. thesis. Gina Cody School of Engineering and Computer Science, Concordia University, Montreal.
- Lin, C.-X. 2022. Guidance for CFD modeling of data centers. ASHRAE Research Project RP-1675, *Final Report*.
- Melikov, A., and J. Kaczmarczyk. 2007. Measurement and prediction of indoor air quality using a breathing thermal manikin. *Indoor Air* 17(1): 50-59. [dx.doi.org/10.1111/j.1600-0668.2006.00451.x](https://doi.org/10.1111/j.1600-0668.2006.00451.x).
- Miller, S.L., and J.M. MacHer. 2000. Evaluation of a methodology for quantifying the effect of room air ultraviolet germicidal irradiation on airborne bacteria. *Aerosol Science and Technology* 33(3):274-295. doi.org/10.1080/027868200416259.
- Miller-Leiden, S. et al. (1996) 'Effectiveness of In-Room Air Filtration and Dilution Ventilation for Tuberculosis Infection Control', *Journal of the Air & Waste Management Association*, 46(9), pp. 869–882. doi.org/10.1080/10473289.1996.10467523.
- Momoi, Y., K. Sagara, T. Yamanaka, and H. Kotani. 2004. Modeling of ceiling fan based on velocity measurement for CFD simulation of airflow in large room. *Proceedings of the 9th International Conference on Air Distribution in Rooms, Coimbra, Portugal*, p. 6.
- NAFA Technical Committee. 2018. *Methods of testing general ventilation air-cleaning devices for removal efficiency by particle size*.
- Ng, L.C., A. Musser, A.K. Persily, and S.J. Emmerich. 2012. Airflow and indoor air quality models of DOE reference commercial buildings. *Technical Note (NIST TN)-1734*. National Institute of Standards and Technology, Gaithersburg, MD.
- Ng, L.C., A.K. Persily, and S.J. Emmerich. 2014. Consideration of envelope airtightness in modelling commercial building energy consumption. *International Journal of Ventilation* 12(4):369-378.
- Ng, L., D. Poppendieck, W.S. Dols, B.P. Dougherty, and S.J. Emmerich. 2018. Balancing energy and IAQ: NIST net-zero energy residential test facility. *ASHRAE Journal* 60(4).
- Pan, J., C. Harb, W. Leng, and L.C. Marr. 2021. Inward and outward effectiveness of cloth masks, a surgical mask, and a face shield. *Aerosol Science and Technology* 55(6):718-733. doi.org/10.1080/02786826.2021.1890687.
- Pardey, Z.M., J.W. VanGilder, C.M. Healey, and D.W. Plamondon. 2015. Creating a calibrated CFD model of a midsize data center. *Proceedings of ASME 2015 International Technical Conference and Exhibition on Packaging and Integration of Electronic and Photonic Microsystems collocated with the ASME 2015 13th International Conference on Nanochannels, Microchannels, and Minichannels*, pp. V001T09A029. American Society of Mechanical Engineers, New York City.
- Qi, D.D., L.L. Wang, and R. Zmeureanu. 2013. Large eddy simulation of thermal comfort and energy utilization indices for indoor airflows. *ASHRAE Conference Papers, Denver, CO*.
- Srebric, J., and Q. Chen. 2001. A method of test to obtain diffuser data for CFD modeling of room airflow. *ASHRAE Transactions* 107(2):108-116.
- Srebric, J., and Q. Chen. 2002. Simplified numerical models for complex air supply diffusers. *HVAC&R Research (now Science and Technology for the Built Environment)* 8(3):277-294. [dx.doi.org/10.1080/10789669.2002.10391442](https://doi.org/10.1080/10789669.2002.10391442).

- Swami, M.V., and S. Chandra. 1988. Correlations for pressure distribution on buildings and calculation on buildings and calculation of natural-ventilation airflow. *ASHRAE Transactions* 94(1).
- Thatcher, T.L., A.C.K. Lai, R. Moreno-Jackson, R.G. Sextro, and W.W. Nazaroff. 2002 Effects of room furnishings and air speed on particle deposition rates indoors. *Atmospheric Environment* 36(11):1811-1819. [doi.org/10.1016/S1352-2310\(02\)00157-7](https://doi.org/10.1016/S1352-2310(02)00157-7).
- U.S. EPA. 2011. *Exposure factors handbook*, 2011 ed. Final Report, Washington, D.C. EPA/600/R-09/052F.
- Van Doremalen, N. et al. 2020. Aerosol and surface stability of SARS-CoV-2 as compared with SARS-CoV-1. *New England Journal of Medicine*, 382(16):1564-1567. doi.org/10.1056/NEJMc2004973.
- VanGilder, J., and M. Seymour. 2014. Seminar 32—developing airflow and thermal models for data centers: Comparing and contrasting the design and operation use cases. *ASHRAE Seminar Recordings, 2014 Annual Conference, Seattle, WA*.
- VanGilder, J.W., and X.S. Zhang. 2008. Coarse-grid CFD: The effect of grid size on data center modeling. *ASHRAE Transactions* 114(2).
- VanGilder, J.W., Z.M. Pardey, and C.M. Healey. 2016. Measurement of perforated tile airflow in data centers. *ASHRAE Transactions* 122(1).
- Walton, G.N., and S. Dols. 2006. CONTAM 2.4 user guide and program documentation. *NIST Interagency/Internal Report* (NISTIR)–7251. National Institute of Standards and Technology, Gaithersburg, MD.
- Wang, H., and Z.J. Zhai. 2012. Analyzing grid independency and numerical viscosity of computational fluid dynamics for indoor environment applications. *Building and Environment* 52:107-118. dx.doi.org/10.1016/j.buildenv.2011.12.019.
- Wang, L.L., and W. Li. 2017. A study of thermal destratification for large warehouse energy savings. *Energy and Buildings* 153:126-135. dx.doi.org/10.1016/j.enbuild.2017.07.070.
- Yan, S., L. Wang, M.J. Birnkrant, J. Zhai, and S.L. Miller. 2022. Evaluating SARS-CoV-2 airborne quanta transmission and exposure risk in a mechanically ventilated multizone office building. *Building and Environment* 219:109-184. doi.org/10.1016/j.buildenv.2022.109184.
- Yakhot, V., and S.A. Orszag. 1986. Renormalization group analysis of turbulence. I. Basic theory. *Journal of Scientific Computing* 1(1):3-51.
- Zhai, J., J. Hertberg, W. Smith, G. Quinn, and J. McNeill. 2013. Experimental investigation of hospital operating room (OR) air distribution (RP-1397). *ASHRAE Research Project RP-1397, Report*.
- Zhai, J.Z., K.A. Hermansen, and S. Al-Saadi. 2012. The development of simplified rack boundary conditions for numerical data center models. *ASHRAE Transactions* 118(2).
- Zhang, Y. 2004. *Indoor air quality engineering*. CRC Press, Boca Raton, FL.
- Zhang, Z., W. Zhang, Z.J. Zhai, and Q.Y. Chen. 2007. Evaluation of various turbulence models in Predicting airflow and turbulence in enclosed environments by CFD: Part 2—comparison with experimental data from literature. *HVAC&R Research* (now *Science and Technology for the Built Environment*) 13(6):871-886. dx.doi.org/10.1080/10789669.2007.10391460.
-

The preparation of this chapter is assigned to TC 4.10